Composite Structures 334 (2024) 117989

Contents lists available at ScienceDirect

Composite Structures

journal homepage: www.elsevier.com/locate/compstruct

Experimental study of bonded, bolted, and hybrid bonded-bolted single lap shear joints with woven CFRP adherends

Mahdi Damghani *, Mohammad Saad Khan, Gary A. Atkinson

School of Engineering, University of the West of England (UWE), Bristol BS16 1QY, UK

ARTICLE INFO

Keywords:
Hybrid joint
Bonded joint
Bolted joint
Single lap shear joint
Composite structures

ABSTRACT

This paper presents an extensive experimental performance study of bonded joints (BJs), only bolted joints (OBJs) and hybrid bonded-bolted joints (HJs). For each joint type, three test configurations are considered: namely, short, medium and long overlap lengths. In each case, the adherends comprise quasi-isotropic twill woven CFRP. For each joint type/overlap length combination, three specimens are tested for statistical representation. HJs demonstrate 1.4, 1.5 and 1.5 times higher failure load and 1.5, 1.6 and 1.9 times higher stiffness than OBJs, for short, medium and long overlap, respectively. In all test cases, HJs outperform BJs except for short overlaps where BJs outperform both HJs and OBJs. OBJs perform poorly in terms of failure load and Hooke's stiffness. Nevertheless, due to bearing deformation at bolt hole locations, OBJs experience higher failure displacements than BJs and HJs leading to a desirable energy absorption mechanism compared to HJs and BJs. This is thanks to the bearing failure mode of the joint despite much lower failure load in OBJs. It was found that increasing the overlap length generally benefits BJs. However, for medium length overlap specifically, HJs show better performance than BJs. Stress–strain behaviours show a linear behaviour for all test groups with significant joint rotation for OBJs compared to BJs and HJs. Failure mechanism studies presented in the paper show that BJs fail in cohesive failure mode for all test groups. OBJs fail in bearing mode, which is followed by net tension failure. OBJs experience matrix cracking and delamination at bolt hole locations. On the contrary, HJs experience considerably less bearing failure at bolt holes due to the load bearing contribution from the adhesive.

1. Introduction

Laminated Carbon Fibre Reinforced Polymers (CFRP) have been used in many structural applications for decades, particularly in aerostructures. This is due to their higher stiffness and strength-to-weight ratios compared to conventional metallic structures such as aluminium alloys, titanium, and steel. Additionally, CFRP materials have the advantage of being resistant to corrosion, which is a commonly reoccurring problem for metallic aircraft components throughout their service life. Furthermore, CFRP benefits from enhanced fatigue performance compared to metallic counterparts [1]. Despite all these benefits, any design and optimisation activity for full scale use of CFRP materials in lightweight and safe structures should include consideration of their weaknesses. Amongst these weaknesses are the difficulties and complexities in repair [2,3] and recycling [4], and that they are prone to transverse impact [5–7].

When repairing laminated composite aerostructures, joining a parent structure to the repair structure is a necessity. Even for an intact structure, otherwise known as a pristine structure, there are many scenarios where joining composite parts together is crucial. For instance, in an aircraft wing, ribs are connected to skin via rib feet in the form of Single Lap Shear joint (SLS). Often, wing composite spars are connected using splice plates in the form of Double Lap Shear joint (DLS). In fact, the wing of an Airbus 380 alone is composed of over 30,000 elements, with approximately 750,000 bolted joints [8]. Thus, joint design in laminated composite structures has been an ongoing concern since the inception of composite materials in structural applications.

At present, there are three main joining methods of composite structures: bonded, mechanically fastened (bolted or riveted) and hybrid (bolted-bonded). In structural adhesive joints, the load in one adherend is transferred through the adhesive layer to another adherend. The load transfer efficiency depends on the joint design, the adhesive characteristics, and the adhesive-substrate interface. The most effective means to transfer loads is through shear in the adhesive. If there is bending in the joint (e.g. due to load eccentricity), peel stresses occur and could cause delamination in the substrate [2]. In this case, adhesives are frequently

* Corresponding author.
E-mail address: mahdi.damghani@uwe.ac.uk (M. Damghani).

https://doi.org/10.1016/j.compstruct.2024.117989
Received 8 September 2023; Received in revised form 17 January 2024; Accepted 19 February 2024
Available online 23 February 2024

modified with rubber or other elastomers, which reduce the adhesive modulus to improve fracture toughness and fatigue life [9]. Additionally, adhesively bonded joints are structurally more efficient than mechanically fastened joints as they perform better in distributing loads, thus eliminating most of the high stress concentration problems seen in bolted joints. However, the use of only adhesives in the joints comes with great deal of risk, particularly for safety critical structures. Amongst such risks are the existence of adherend surface contamination that could lead to a weak joint [10]. Adhesives are also vulnerable to environmental factors. The main environmental threats are related to the effect of temperature and moisture absorption (humidity) which can affect the strength and durability of the joints [11]. Lack of control of the surface roughness of adherends [12] and maintaining a constant bond-line thickness [13] are amongst other disadvantages of bonded joints. These make it difficult to obtain aircraft certification requirements where bonded joints are used.

On the other hand, the use of only fasteners (bolts, rivets, and pins) to join composite structures, is not ideal despite being the dominant method in industry. Although mechanically fastened joints and components are easy to disassemble and inspect [14], the stress concentration around the fastener holes in composite structures is much higher than those in their metallic counterparts and there is a strong dependency of stress concentration on the stacking sequence of composite laminates [15]. Furthermore, plasticity in ductile metals relieves the stress concentration and causes it to have a small effect on the net failure stresses, but such ductile behaviour does not exist for laminate composite plates. In other words, the efficiency of brittle composite bolted joints is lower than that of metallic bolted joints. Although the most common failure mode for bolted joints is bearing failure, the strongest possible failure mode per unit laminate width is always the net-section tension [16]. Finally, fasteners add extra undue weight to the structure. In the case of aerospace industry, they are expensive as they are made of titanium to avoid galvanic corrosion.

Based on the above, the quest for alternative yet reliable means of joining safety critical composite structures continues to this date. Amongst such methods is the hybrid use of fasteners and adhesives in the form of a Hybrid Joint (HJ) to combine the benefit of both and diminish the disadvantages of each individual component. This topic has been studied for more than thirty years. It is understood that, generally, HJs provide better static and fatigue performance compared to either of bonded or mechanically fastened joints [17].

Thus, the aim of this paper is to carry out an extensive experimental study to investigate the behaviour of three configurations of SLS joints using woven CFRP adherends and brittle adhesive. The joints studied in this work are Bonded Joints (BJs), Only Bolted Joints (OBJs) using two bolts and Hybrid (bonded-bolted) Joints (HJs) considering various overlap lengths and load eccentricity under uniaxial tensile loading. Thus, this paper bridges the gap in knowledge in the literature with the following novel aspects:

- Unlike many studies in the literature, the effects of load eccentricity on the joint performance are considered.
- The impact of overlap length on the overall joint performance is studied.
- Edge distance design rules as outlined in the literature and practiced in industry are respected.

The remainder of this paper is organised as follows. In section 2, an in-depth background study is presented. The applied methodology is provided in section 3, which includes material selection and properties, and information on the manufacturing of specimens and joints. Results of a detailed behavioural study of the joints is presented in section 4 in the form of force–displacement graphs, stress–strain curves, and examination of failure modes. Finally, conclusions and future works are provided in section 5.

2. Literature survey

This section surveys the current state-of-the-art in HJs in chronological order and identifies parameters that affect both static and fatigue performance of such joints.

Fu and Mallick [18] carried out both static and fatigue experiments of SLS joints in composites. The purpose of their study was to examine the effects of washer type as well as washer geometry on the performance of HJs. They reported that the HJs gave better static as well as fatigue performance than adhesive joints. The primary reason for this was associated with the clamping force of bolts that reduced adhesive peel stress delaying the adhesive failure.

Kelly [19] investigated the distribution of load within hybrid SLS in composites via 3D nonlinear Finite Element Analysis (FEA) and experimental validation. He isolated the effect of load eccentricity and, hence, the resulting bending moment in the joint. This established that the load transfer mechanism in the joint was correlated to adherend thicknesses, adhesive thickness, overlap length and bolt pitch distance. Kelly concluded that the benefit of adding bolts to a bonded joint is greater if the joint is flexible either because of the adhesive material or joint design. However, the method could also provide performance improvements for a wide range of joints in adverse environments with both elevated temperature and moisture reducing the performance of the adhesive. Furthermore, it was suggested that the addition of bolts to a bonded joint improves the damage tolerance, with the bolt preventing catastrophic failure of the joint through separation of the adherends.

Matsuzaki et al. [20] proposed a bolted/co-cured hybrid joining method, and experimentally investigated the joint strength under static tensile and fatigue loading. They considered three joint configurations for a SLS joint comprising of two adherend types of aluminium and GFRP: co-cured, bolted and hybrid of both. The HJs had 1.84 times higher maximum shear strength and a quarter of the standard deviation compared with the adhesive failure strength of the co-cured joints. Hybrid joints also demonstrated much higher fatigue strength compared to bolted joints thanks to less stress concentration and undamaged glass fibres.

Esmaeili et al. [21] studied the effects of the bolt tightening torque on the fatigue strength of DLS bolted and HJs via experimental and numerical analysis for metallic adherends (2024-T3 aluminium alloy). It was revealed that increasing the tightening torque or clamping force on the joint led to improved fatigue resilience. It was also observed that the HJs had longer fatigue lives in comparison with the simple bolted joints.

Bodjona et al. [22] argued that only few bonded-bolted joint designs experience load sharing between the fastener and the adhesive. This was evident from several experimental studies in which the initial failure of HJs corresponded to the bonded joint strength, after which the joint behaved like a bolted joint. Such distinct behaviour is indicative of little or no load-sharing. Thus, they developed a computational model to predict the load sharing in SLS HJs having only a single bolt considering clearance, contact, material nonlinearity and bolt clamp-up. Significant load sharing was observed, with the bolt carrying up to 40% of the overall applied load. The model predictions were found to agree well with both the experimental measurements and a detailed 3D FEA. In a later study [23], they performed a comprehensive global sensitivity study and concluded that for substantial load sharing ($> 10\%$) to occur, the adhesive overlap must fully plasticise. For designs in which this did not occur, no substantial load sharing was observed at the medium or high loads. Adhesive thickness and bolt-hole clearance were the next most important factors for load sharing.

Chowdhury et al. [24] considered three joint configurations with a focus on aerospace applications with the same joint types as considered in this paper (BJ, OBJ and HJ). They reported that for bonded joints, larger bond areas resulted in greater joint stiffness. However, for the HJs, they confirmed the findings of [22,23] and suggested that the joint load share of the fasteners was negligible, but the fasteners were critical in reducing the peel stress within the bond-line of a HJ. In addition, the

fasteners were vital in supressing crack growth followed by adding residual strength to the joint once the bond-line had failed. Most notably, they highlighted that the fatigue life of HJs was significantly higher than non-hybrid ones, particularly in those with more rows of fasteners. This was mostly associated to the added clamping pressure provided at the ends of the overlap hindering rapid crack growth.

Cruz et al. [25] presented a design of experiments methodology to analyse the performance of bolted-bonded composite joints by considering several design variables at the same time. They considered both high and low modulus adhesives. It was reported that the static strength of the HJs increased by 66% and 47% compared to the bolted and bonded joints with low modulus adhesive, respectively. Like previous works mentioned above, they observed that the failure process in the adhesive was accompanied by the presence of crack initiation in the adhesive before the joint maximum strength was reached. The propagation of the crack was delayed due to the presence of the bolt, which thus improved the performance of the joints at maximum load.

The effects of material type and thickness of adherends for SLS HJs was examined by Zaroug et al. [26]. They used teflon shims to control the bond-line thickness ($0.2mm$) between aluminium alloy (AL6061 and AL7075) adherends of varying thicknesses ($2mm$, $4mm$ and $6mm$). It was found that HJs in thicker adherents had higher failure loads. They observed that the maximum load that the SLS joint carried did not change significantly for either joint type. This was attributed to the fact that the use of stiff adhesive did not allow adhesive-bolt load sharing. More interestingly, the amount of energy absorbed (EA) in the hybrid joint, i.e. area under force–displacement curve, was nearly equal to sum of the EA for both joint types, i.e. the bonded joints and the bolted joints, when stiffer AL7075 adherends were used. However, this was not the case for the joints with the thicker AL6061 adherends. Thus, the efficiency of HJs is dependent on the mechanical behaviour of the adherend materials.

Most of the work mentioned so far, endeavoured to eliminate the load eccentricity inherent in SLS joints. However, this scenario is not representative of real-life applications, particularly that of aerostructures. Amongst few works that included load eccentricity in their study was the work of Li et al. [27]. They indicated that the secondary bending was serious in the SLS composite joints. Increasing the ratio of plate width to fastener diameter could decrease the effect of the secondary bending and change the fracture mode from bearing failure to net-section failure.

Mehrabian et al. [28] provided a unique understanding of HJs. They used 3D digital image correlation (3D-DIC) to explain the tensile behaviours of SLS OBJs and HJ via measurement of strain distribution and secondary bending/twisting, as well as the balance between bypass and bearing loads in woven CFRP adherends. However, they reduced the load eccentricity effects via their test set-up. They reported that the strength of HJs was almost twice as much as OBJs in cross-ply than quasi-isotropic stacking sequence. Thinner adherends outperformed the thicker ones as geometric load eccentricity, and therefore adhesive peel stresses, reduced. Hybridization eased the all-round strain/stress distribution as well as the bearing action, noticeably relieving the stress concentration around the holes, thereby helping cross-ply joints sustain more strength than quasi-isotropic by approximately 13.5%.

Romanov et al. [29] studied the effect(s) of overlap length, bolt edge distance and bolt pitch on the tensile static strength of HJs. The longer overlap length was beneficial to the reduction of adhesive stresses but was detrimental to bolt-adhesive load sharing. The reduction in the ratio of overlap length to bolt pitch led to an increase in static strength.

Jiang et al. [30] showed that adhesive can greatly improve the state of the tension–compression area distribution around the hole edge, thus reducing the hole side compression area. In the case of a hybrid bolted-bonded joint, the structure was more stable, with less hole edge bearing failures. The load was effectively transferred to the plate in such cases, and the strain value increased. Unlike bolted joints, the strain distribution of the hybrid joint was more uniform, and the structural strength and stiffness was effectively improved. Li et al. [31] also conducted a detailed experimental study of SLS joints considering many design parameters such as the stacking sequence, the number of bolts (one or two), the diameter of bolts, the introduction of adhesive, and the geometric dimensions under static tensile loading. Amongst the conclusions were an increase of load and bearing strength in HJs compared to bolted ones, particularly for quasi-isotropic lay-up. Additionally, the HJs still had the bolt bearing capacity after the first brittle failure. It was suggested that the HJs could be used as a safety structure to improve the damage tolerance of the joint structure. From this perspective, the contribution of the bolt in the HJ was considered as a redundant load path to improve structural safety.

A summary of some of the existing research and their key findings is provided in Table 1.

It has been found that the overall static and fatigue strength of HJs exceeds that of bonded or bolted joints. Only few of the previously mentioned works consider load eccentricity. Moreover, the bulk of studies focus on single bolt hybrid joints. It is worth noting that the majority of aerostructures not only have significant secondary bending moments (resulting from load eccentricity) within SLS joints but also require multiple fastener configurations to transfer significant aerodynamic loading. Thus, there is still a substantial lack of knowledge regarding the behaviours of multi-bolt HJs. The literature identifies many geometric factors that affect overall static and fatigue performance of HJs amongst which are

- Material type of adherends [26],
- Stacking sequence of composite adherends [28],
- Thickness of adherends [28,26],
- Material type of adhesive (ductile/brittle and high/low modulus) [33],
- Thickness of adhesives [19],
- Fastener hole clearance [19,20,25],
- Number and size of fasteners [31],
- Overlap length [32],
- Overlapping pattern, i.e. SLS, DLS or Single Strap Butt (SSB) joint [32]

However, the effects of overlap length have received little attention. Thus, there is limited experimental work and understanding on how overlap length [29,32] impacts the behaviour of multi-bolt HJs in woven CFRP including the effects of load eccentricities. Thus, this paper aims to determine the relative benefits and limitations of combined overlap length and load eccentricity in a SLS joint configuration respecting existing rules for bolt edge distances in composite laminates.

3. Methodology

This section describes the experimental methodology used to investigate the various properties of BJs, OBJs and HJs and their relative strengths and weaknesses.

3.1. Materials

The materials used in this study are twill woven pre-impregnated carbon fibre (AX-5180) with the mechanical properties given in Table 2. Carbon pre-pregs consist of 54 % fibre by volume (60 % by weight). This material system is selected for this study as appropriate data for design has previously been generated and published by the authors [34,35].

The brittle adhesive used is XA120 150 g (areal weight of 150 g/m^2) film with minimum and maximum cure temperatures of 80 $^{\circ}C$ and 120 $^{\circ}C$, respectively. Key properties are provided in Table 3.

The fasteners are M10 and are made of steel with mechanical properties provided in Table 4.

Table 1
Summary of work in the literature on HJs.

Authors	Loading	Procedure	Adherends	Joint configurations	Some of key findings
Bodjona et al. [22,23]	Tensile (static)	Experimental & numerical (FEA)	CFRP	SLS: Bonded/bolted (1) *	For load sharing, adhesive plasticity is crucial. Difficulty in obtaining load sharing at low loads with adhesive taking most of the load. Adhesive thickness and bolt-hole clearance are the next most important factors.
Chowdhury et al. [14]	Tensile (static & fatigue)	Experimental	CFRP	DLS: Bonded Riveted (3 & 6) ** Bonded/bolted	HJ had enhanced static strength and fatigue resistance. Rivets arrested rapid crack growth and prevented sudden catastrophic failure.
Chowdhury et al. [24]	Tensile (static & fatigue)	Experimental & numerical (FEA)	CFRP	Stepped scarf: Bonded Bolted (3 & 5) Bonded/bolted	Enhanced static strength and fatigue life of HJs.
Cruz et al. [25]	Tensile (static)	Experimental	CFRP	SLS: Bonded/bolted (1)	The strength in the HJ was mainly driven by the adherend thickness and adhesive modulus, with a combined effect of 77.1% at the first failure point of the adhesive layer and 67.1% at maximum strength.
Zaroug et al. [26]	Tensile (static)	Experimental & numerical (FEA)	Aluminium alloys AL7075 and AL6061	SLS: Bonded/bolted (1)	The amount of energy absorbed in HJ was nearly equal to sum of that of both bonded and bolted types, for stiffer adherend AL7075.
Li et al. [27]	Tensile (static)	Experimental	Carbon-fibre reinforced bismaleimide (BMI) resin composite	SLS: Bonded Bolted (1) Bonded/bolted	The bolt in HJ was effective in enhancing the tensile capacity of the specimen after the adhesive failure, but the secondary bending was serious.
Romanov et al. [29]	Tensile (static)	Experimental & numerical (FEA)	CFRP	SLS: Bonded/bolted (2)	Load sharing was facilitated by shorter joint overlap length and smaller bolt-edge distance for two-bolt HJ.
Jiang et al. [32]	Tensile (static)	Experimental	CFRP	SLS: Bonded Bolted (4) Bonded/bolted SSB ***: Bonded Bolted (4) Bonded/bolted	The strength of a bonded joint can be greater than that of an HJ with a high-performance adhesive. HJs improved structural stiffness and strength compared to bolted ones.

*Number in parentheses shows the number of bolts used in the joints.
** They used staggered and square rivet patterns applicable to aerospace applications.
*** Single strap butt joint.

Table 2
Mechanical properties of both woven CFRP (AX-5180) fabric plies [6,34].

Mechanical properties	Units	AX-5180 CFRP
$E_{11} = E_{22}$(elastic modulus in 1 & 2 directions)	MPa	67,094
G_{12}(shear modulus in plane 1–2)	MPa	4831
S_t(tensile strength)	MPa	595
S_c(compressive strength)	MPa	393
S_S(shear strength)	MPa	87
Strain to failure	Strain	0.01
ϑ_{12}(Poisson's ratio)	N/A	0.04
t_{ply}(cured ply thickness)	mm	0.22

Table 3
Mechanical properties of adhesive film XA120.

Mechanical properties	Units	XA120
E(modulus of elasticity)	MPa	1644
G(shear modulus) *	MPa	610
S_t(tensile strength)	MPa	30
S_S(shear strength) **	MPa	18
ϑ_{12}(Poisson's ratio)	N/A	0.35

For the fasteners, stainless steel washers (DIN 125) on both sides of the M10 bolts (DIN 933 class 12.9) and hexagonal stainless-steel nuts (DIN 934) are used.

Table 4
Mechanical properties of M10 steel fastener [41,42].

Mechanical properties	Units	12.9 grade steel bolt
E(modulus of elasticity)	MPa	210,000
F_u(ultimate strength)	MPa	1220
F_y(yield strength)	MPa	1100
F_s(shear strength)	MPa	813
ϑ_{12} (Poisson's ratio)	N/A	0.30

*estimated from $G = E/2(1+\vartheta_{12})$ based on [36].
**approximated from $0.5S_t + \mu$ for brittle adhesives where μ (standard deviation) is taken as an average of data from [37–40].

3.2. Preparation of CFRP adherend laminates

Laminates representing adherends are initially hand laid to form a plate and cured in a heated press for an hour at $120^{\circ}C$ under $100psi$ pressure. The adherends have 12 plies with Quasi-Isotropic (QI) lay-up of $[\pm 45_3/0_3/0_3/\pm 45_3]$. QI SLS joints were chosen based on [28], which showed these have better bearing performance than cross-ply laminates. Note that, since the material used in this study is woven fabric, 0° plies also include fibres at 90°. The specimens are then abrasively cut into strips of $50mm$ width using a bandsaw cutter having varied overall lengths and gauge lengths depending on the joint overlap length (see section 3.3).

3.3. Joint preparation

3.3.1. Joint geometry

Three groups of tests are manufactured: Group 1 (G1), Group 2 (G2) and Group 3 (G3). For each group, a specific overlap length is considered:35t, 45t and 60t for G1, G2 and G3, respectively, where t is the thickness of adherends, i.e. $t = 12 \times 0.224mm = 2.688mm$. The choice of overlap length is based on existing rules for composite stepped scarf joints as detailed in [2]. Each group considers three joint configurations: bonded (BJ), only bolted (OBJ) and hybrid bonded/bolted (HJ) joints. Three specimens of width 50mm are manufactured for each configuration in the group, totalling 9 specimens each for G1, G2 and G3. For BJ and HJ configurations, two M10 bolts with shank diameter of 10mm (D) are positioned at the recommended edge distance (e) for laminated composites ($e = 3D = 3 \times 10mm = 30mm$). This enables the bolts to fully develop their bearing strength and avoid interference of free edge with stresses around the fastener hole avoiding premature failure of the joint [43]. The choice of bolt size is determined to ensure the total failure shear load in two M10 bolts are higher than failure load of each adherend as obtained in [2]. In other words, the joint is designed so that the joint failure does not take place in the bolts. The bolt pitch is generally considered to be $\geq 4D$ except for G1, where bolt pitch of 3D is used as 4D is not possible given the existing edge distances. The minimum bolt pitch of 4D is designed to allow full development of bypass load without any stress interference from the next neighbouring bolt [43]. See Fig. 1-Fig. 3 for detailed illustrations of the geometry of each configuration.

3.3.2. Preparation of joint specimens

The BJs are created by lightly sanding the adherends. The faying surfaces are washed with distilled water and cleaned with alcohol. The adhesive film XA120 is cut to size based on overlap length (see Fig. 4a) and placed between the two adherends. It is assumed that this manufacturing process under controlled conditions will provide an adhesive layer with uniform thickness for all samples. Specimens are then placed in a vacuum bag under 1 bar of pressure (Fig. 4b). The vacuum bag is then placed in the heated press at temperature of 120$^{\circ}C$ for 1 hour (Fig. 4c). The press is used for the heating element only so does not apply unnecessary pressure. Cured BJ specimens are cleaned before aluminium tabs are attached using araldite and clamps as shown in Fig. 4d. Note that, since the thickness of the aluminium tabs is equal and placed symmetric about the mid-plane of adherends, this does not alter the load eccentricity and the resulting nonlinearity in the joints.

The OBJs are manufactured by first marking the hole locations

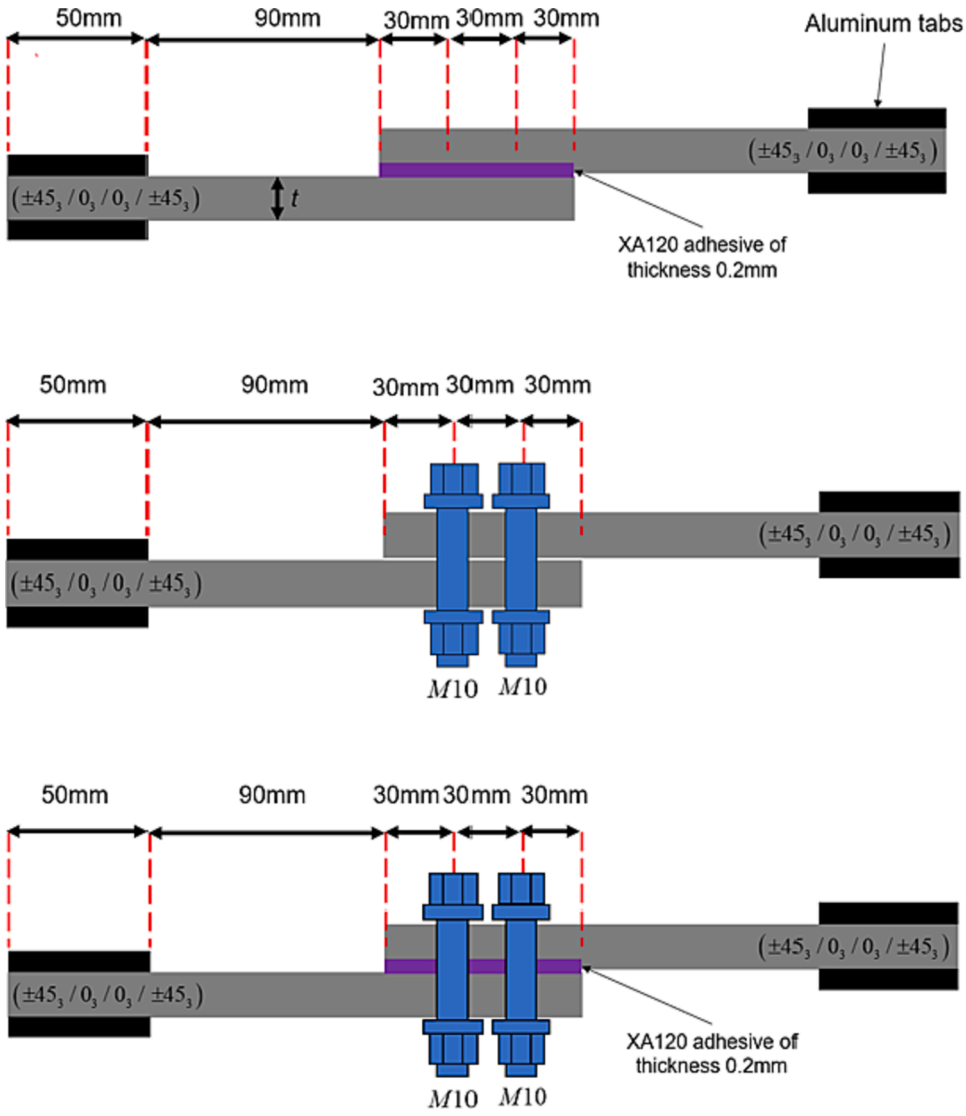

Fig. 1. Schematic of G1 having overlap length $\approx 35t$ with three joint configurations of BJs, OBJs and HJs (width of each adherend is 50mm and 0° fibre orientation is defined to be in the tensile loading direction).

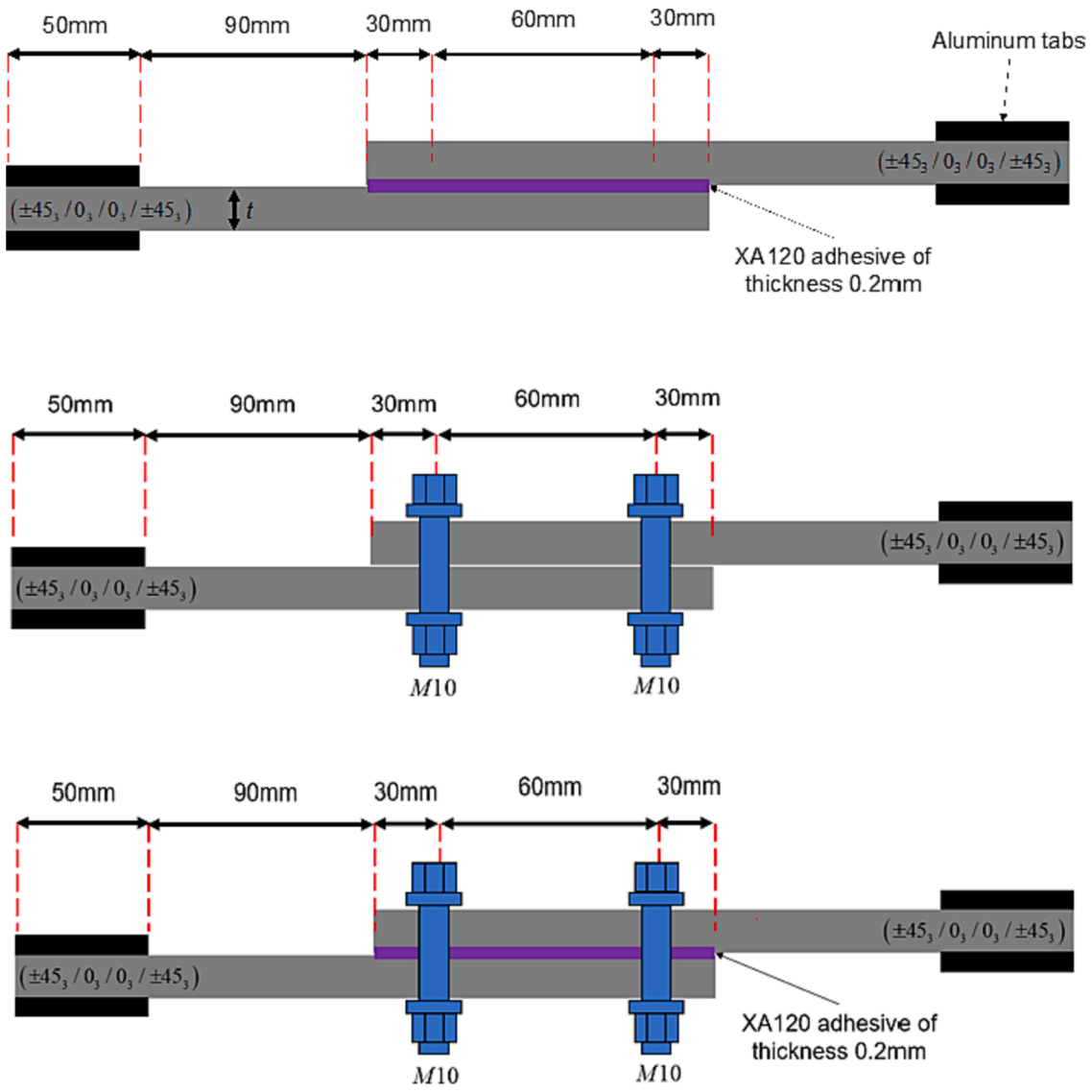

Fig. 2. Schematic of G2 having overlap length $\approx 45t$ with three joint configurations of BJs, OBJs and HJs (width of each adherend is 50*mm* and 0° fibre orientation is in the tensile loading direction).

(Fig. 5a). Both adherends are attached using removeable paper tape. Adherends are placed on a wooden panel and fixed in position using steel clamps (Fig. 5b). A fixed drill with drill bit of diameter 10*mm* is driven down to a pre-set penetration depth. Stainless steel washers (DIN 125) are used on both sides of the M10 bolts (DIN 933 grade 12.9) and hexagonal stainless-steel nuts (DIN 934) are used to fasten both adherends using the recommended clamping torque of 6*N.m* (Fig. 5c) [34]. In aerospace applications, the bolt is pre-loaded with 50% of its tensile strength, i.e. 20*N.m* in the case of M10 bolt of this study. However, to have comparative results with that of HJ, the preload was kept at 6*N.m* for this research. This value was chosen so that the compressive stress within the cured adhesive film resulting from fastener pre-load does not lead to compressive failure of the adhesive film in the HJs. A hand calculation was carried out to convert torque load (6*N.m*) into equivalent bolt axial force (3036*N*). The bolt axial force was divided by the washer area ($(20^2/4 - 10^2/4)\pi = 235.62mm^2$) yielding compressive stress in the adhesive underneath the bolt ($3036/235.62 = 13MPa$). The compressive stress was then multiplied by 2 to account for contact stresses (triangular stress distribution under the washer as opposed to uniform rectangular distribution leading to contact stress of $2 \times 13 = 26MPa$). The compressive stress of the adhesive was then conservatively compared against adhesive tensile strength (30*MPa*) to ensure no adhesive failure took place under the given bolt torque ($26MPa < 30MPa$).

The HJs are initially manufactured similarly to the OBJs, i.e. marking the fastener hole locations and drilling.

For both HJs and OBJs, an interference-fit of $I \approx 2\%$ is used where the level of interference is defined as

$$I(\%) = \frac{d_b - d_h}{d_h} \times 100$$

where d_b and d_h are bolt and bolt hole diameters, respectively. This level of interference-fit, i.e. 2%, has proven to improve load sharing in the HJs [44].. Furthermore, the interference fit approach not only creates minor compressive stresses around the hole intended to close any potential drilling induced cracks but also lowers the stress concentration factor at the bolt hole [45].

It should be noted that the use of drill bits for creating holes in composites is not the optimal method. However, in the current study, the use of drill bits is the only available option to the authors. Alternatively, the use of other cutting processes such as laser beam cutting, water jet machining and electro-discharge machining could provide holes with less likeliness of process-induced defects [46]. Adhesive film

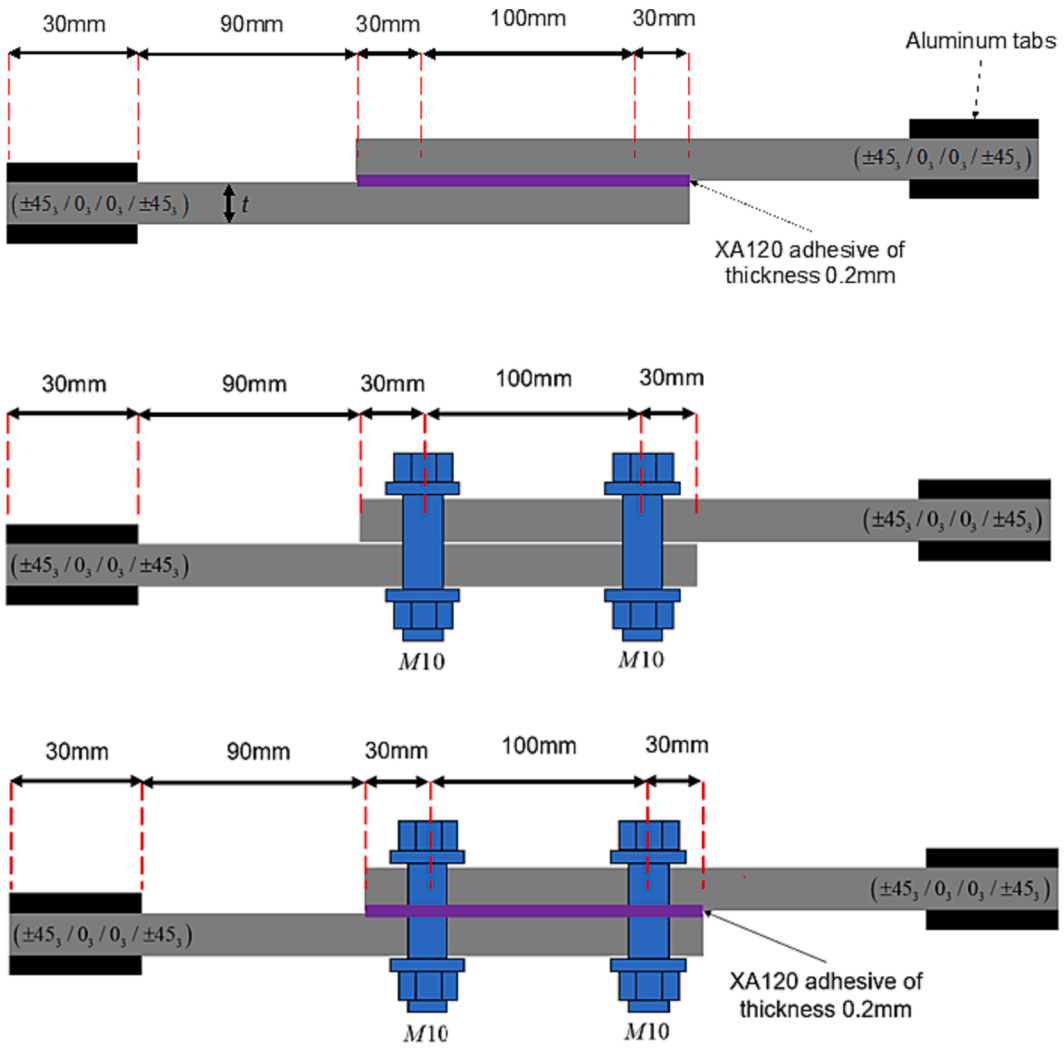

Fig. 3. Schematic of G3 having overlap length $\approx 60t$ with three joint configurations of BJs, OBJs and HJs (width of each adherend is 50*mm* and 0° fibre orientation is in the tensile loading direction).

XA120 is cut to size and placed between the adherends (see Fig. 6a). The fasteners are positioned in place and are tightened lightly using torque of $3N.m$ [30] to provide sufficient clamping for the adhesive curing stage (Fig. 6b). The assembled joint is then placed in a vacuum bag in an oven at temperature of $120^{\circ}C$ for 1 hour (see Fig. 6c), as per the BJ case. Once the adhesive is cured and cooled down, the fasteners are tightened to the final torque of $6N.m$.

3.4. Experimental set-up

To have statistically representative data, three coupons of each joint configuration are tested in uniaxial tension using a $100kN$ capacity INSTRON tensile machine at a speed of $2mm/min$. Two each of BJ, OBJ and HJ coupons in each test group (G1, G2 and G3) are tested for failure loads and displacements with the other one reserved for strain gauging. The gauges are placed in three locations. For OBJ and HJ, these locations are shown in Fig. 7 (left): in the middle of the specimen (SG1), at the edge of the overlap length on the top adherend (SG2) and opposite to SG2 (SG3) on the other adherend. For BJs, SG1 is in the middle of specimen, SG2 and SG3 are on the opposite sides at the far end of overlaps as shown in Fig. 7 (right). The strain gauges have grid resistance of $120.0 \pm 0.3\%\Omega$. For all specimens, the strains in the laminates away from the joint close to the loaded end are obtained using second generation INSTRON Advanced Video Extensometer (AVE 2) Non-contacting Video Extensometer. For this, the movement of two white dots at certain distances apart are measured during the test. This strain measuring technique allows the measurement of average strains throughout the test up to the point of failure without the need to pause the test for removing a physical extensometer. Hence, AVE 2 not only provides more accurate and representative results than conventional extensometers but also eliminates the effect of operators on strain results leading to more consistent and repeatable results. The reason for positioning the strain gauges alongside AVE 2 was to observe the flow of stress and strain paths from the plates into the joint.

4. Results and discussions

This section provides results and discussions on force–displacement response (section 4.1), stress–strain response (section 4.2) and failure modes (section 4.3) of specimens for each test configuration G1, G2 and G3.

4.1. Force-displacement response

Force-displacement graphs for G1 (short overlap length of $35t$) joints are provided in Fig. 8 and the characteristic results, i.e. maximum force, maximum displacement, Hooke's stiffness (slope of linear portion of force–displacement graphs) and absorbed energy (area underneath

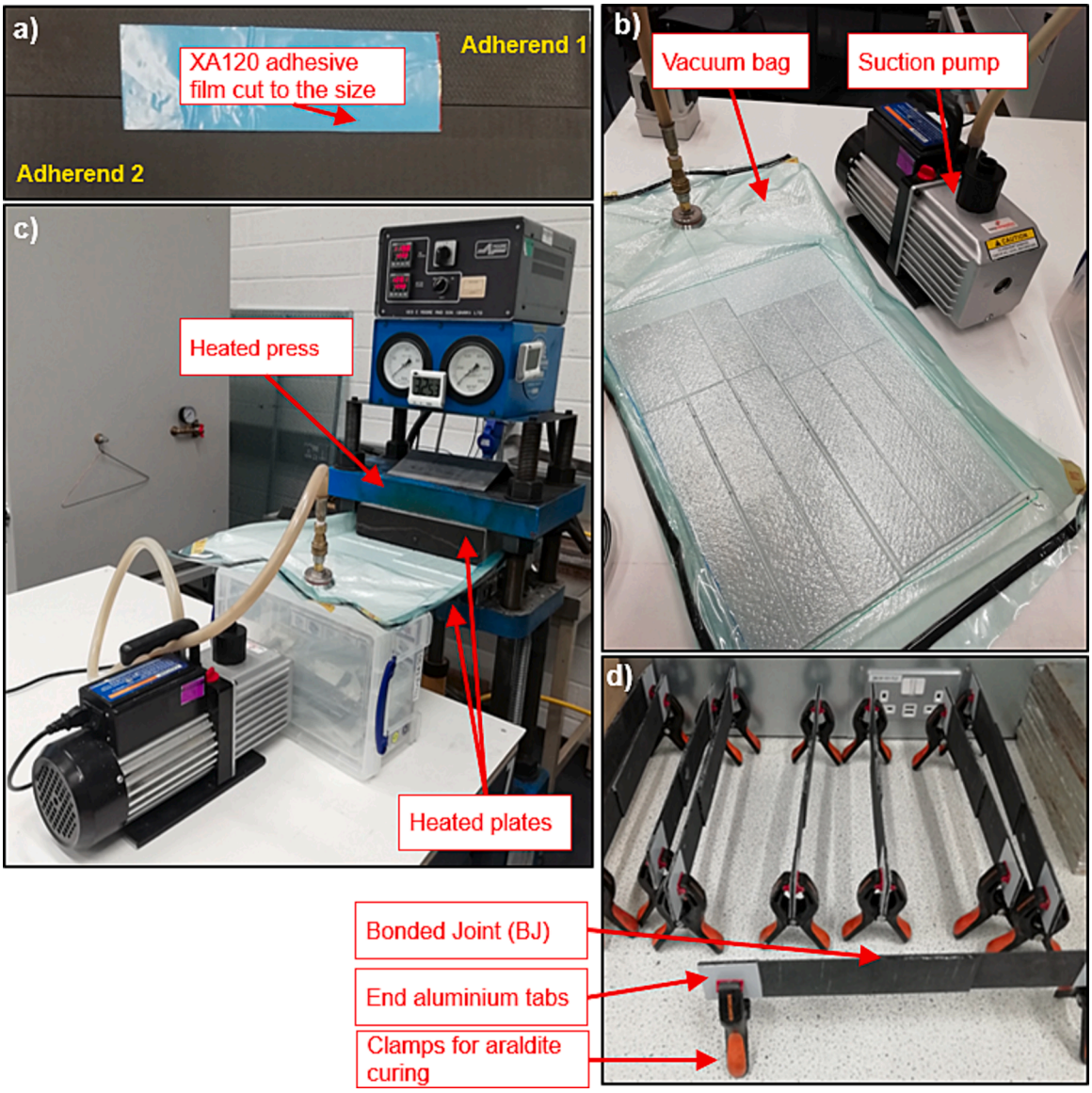

Fig. 4. Sequence of activities in the manufacture of BJs, a) cutting the XA120 film and adherends to size, b) vacuum bagging the joint assembly, c) placing the vacuum bag in heated press and d) applying the end tabs.

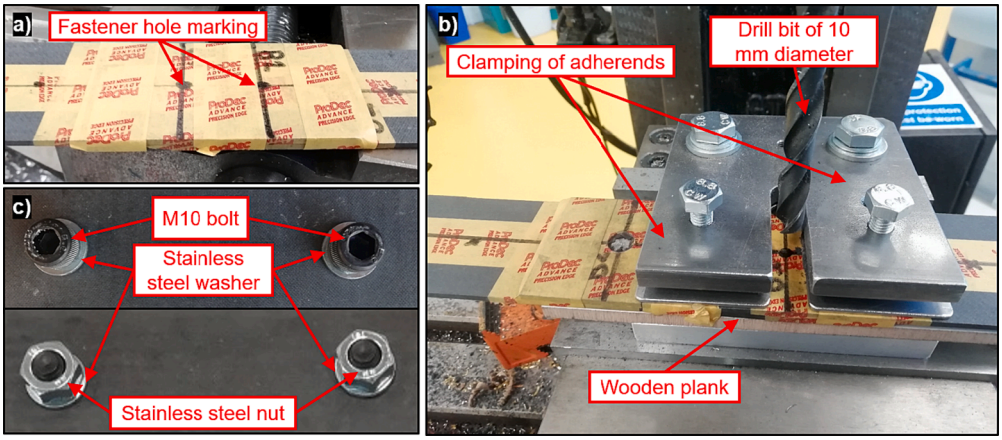

Fig. 5. Sequence of activities in the manufacture of OBJs, a) marking the fastener hole locations, b) drilling the fattener holes, c) placing the fasteners and tightening to the torque of $6N.m$.

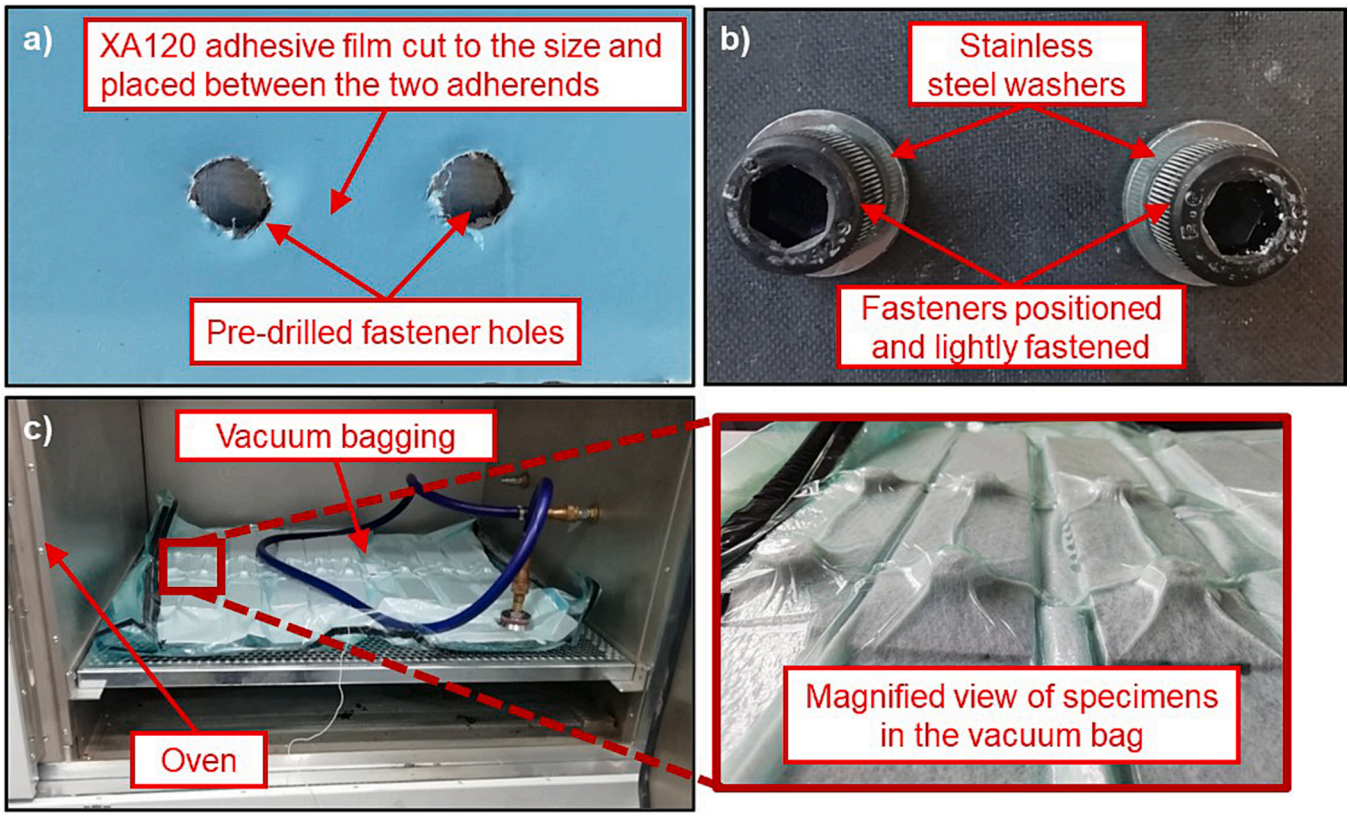

Fig. 6. Sequence of activities in the manufacture of HJs, a) cutting XA120 film to size, b) lightly tightening fasteners using $3N.m$ torque, c) placing the vacuum bag in the oven.

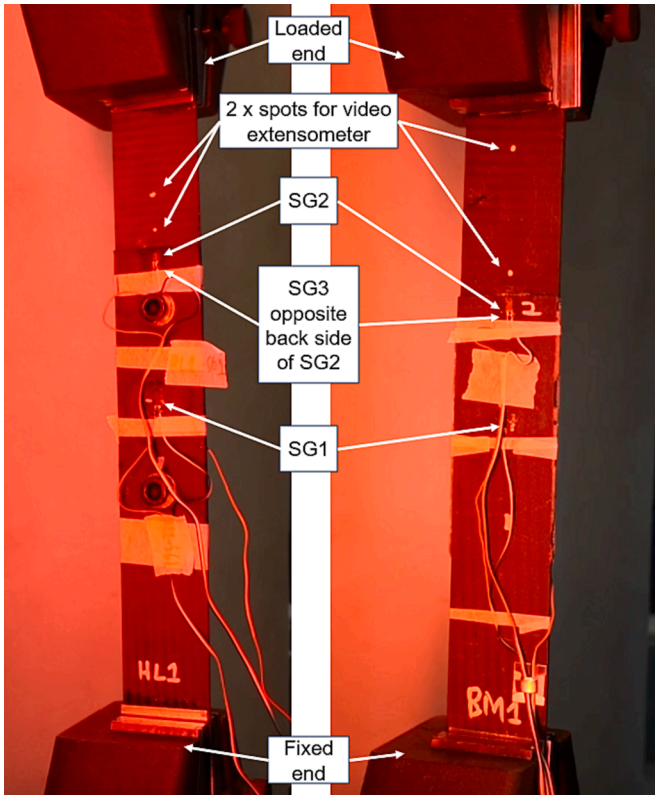

Fig. 7. Experimental test set up and position of strain gauges for OBJs and HJs (left) and BJs (right).

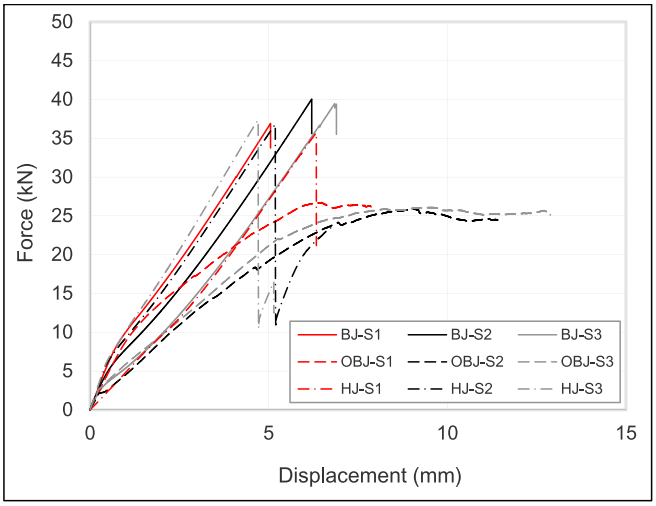

Fig. 8. Force-displacement graph of G1 joints for BJ, OBJ and HJ.

force–displacement graphs), for each specimen in the group are tabulated in Table 5. The average results are normalised to the respective values of OBJ and shown graphically in Fig. 9. The standard deviation of each parameter is normalised to the average value and are shown as error bars in Fig. 9.

As shown in Fig. 8, both BJs and HJs demonstrate a linear force–displacement behaviour. However, for HJs, after the peak force of the linear portion is reached, the bonded area fully fails (see section 4.3) and fasteners begin to resist the existing load in a similar manner to OBJs. Hence, the force–displacement behaviour changes to become fully nonlinear after the force drop. In other words, the HJ behaviour is

Table 5
Maximum force, displacement and Hooke's stiffness of G1 joints.

Specimen	Maximum Force (kN)	Maximum Displacement (mm)	Hooke's Stiffness (kN/mm)	Absorbed Energy (J)
BJ-S1	36.90	4.77	6.516	49.01
BJ-S2	41.70	6.21	5.593	66.97
BJ-S3	40.73	6.91	4.724	68.67
Average	39.78	5.96	5.611	61.55
SD	2.54	1.09	0.896	10.90
Average ± SD	39.78 ± 2.54	5.96 ± 1.09	5.611 ± 0.896	61.55 ± 10.90
OBJ-S1	26.71	7.56	4.247	73.71
OBJ-S2	25.90	11.29	3.980	103.98
OBJ-S3	26.07	12.79	3.876	128.18
Average	26.23	10.55	4.034	101.96
SD	0.43	2.70	0.191	27.29
Average ± SD	26.23 ± 0.43	10.55 ± 2.7	4.034 ± 0.191	101.96 ± 27.29
HJ-S1	35.67	7.89	5.332	60.38
HJ-S2	36.79	6.40	6.257	64.71
HJ-S3	37.30	4.79	7.081	49.10
Average	36.59	6.36	6.223	58.07
SD	0.83	1.55	0.875	8.06
Average ± SD	36.59 ± 0.83	6.36 ± 1.55	6.223 ± 0.875	58.07 ± 8.06

initially similar to a BJ until the failure of the bonded area, at which point it becomes more like that of an OBJ but does not manage to reach the failure load of OBJs. This pattern of behaviour is indicative of no-load sharing between the adhesive and the fasteners. On the other hand, OBJs behave almost linearly at the start of the test. However, at displacement of $\approx 5mm$, their force–displacement behaviour becomes nonlinear. This behaviour was observed by Jiang et al. [30] where their bolted joints followed a nonlinear load–displacement path. It is worth noting that in [30], the most nonlinear force–displacement behaviour was associated with bolted joints in which adherends were purely made of 12 of $\pm 45^{\circ}$ cross-plies.

As shown in Fig. 9 for G1, BJs and HJs endure 1.5 and 1.4 times higher tensile failure load than OBJs. Furthermore, the Hooke's stiffness of BJs and HJs are 1.4 and 1.5 times higher than OBJs. It can be concluded that for short length overlap joint configuration, BJs marginally outperformed the HJs and significantly outperformed OBJs with higher load bearing capacity. In other words, it can be inferred that stress concentration from bolts and reduction of net cross-sectional area due to bolt holes in HJs worked to the detriment of the joint performance. Comparison of absorbed energy for each joint configuration in G1, suggests that OBJs have superior ability to absorb energy. In fact, the energy absorption capacity of both BJs and HJs is only 60% of the OBJs. As shown later, in section 4.3, this is due to the nature of bearing failure mode and subsequently large displacement at failure of OBJs in which composite adherends deform in bearing mode under constant load. This is also shown in force–displacement graphs (Fig. 8) after displacements of $\approx 7mm$. In other words, the failure of OBJs is gradual and unlike BJs and HJs, does not involve sudden failure of the joint. This type of failure is desirable in safety critical structures such as aerostructures.

Force-displacement graphs of G2 (medium overlap length of $45t$) joints are provided in Fig. 10 and the characteristic results for each specimen in the group are tabulated in Table 6. The average results are normalised to the respective values of OBJ (including the error bars) and shown graphically in Fig. 11.

Based on Fig. 10, like G1, both BJs and HJs demonstrate a linear force–displacement behaviour for G2. On the other hand, OBJs behave linearly at the start of the test. However, at displacement of $\approx 6.5\,mm$, their force–displacement behaviour becomes nonlinear. BJs and HJs endure 1.3 and 1.5 times higher tensile failure load than OBJs. Furthermore, the Hooke's stiffness of BJs and HJs are 1.7 and 1.6 times higher than OBJs. Hence, for medium overlap length joint configuration, the load bearing ability of HJs outperforms that of BJs and OBJs. Comparison of absorbed energy for each joint configuration in G2, implies that OBJs have superior ability to absorb energy. In fact, the energy absorption capacity of both BJs and HJs is only 40% that of the OBJs. Again, this is due to the bearing failure mode of OBJs in which composite adherends are deforming in bearing under constant load. This is also shown in the force–displacement graphs (Fig. 10) after displacements $\approx 7mm$. In other words, the failure of OBJs is gradual and unlike BJs and HJs, does not involve sudden failure of the joint.

Results of G3 (long overlap length of $60t$) joints are provided in Fig. 12 and Fig. 13 with characteristic results tabulated in Table 7 following a similar format to the results of G1 and G2.

Based on Fig. 12, like G1 and G2, BJs and HJs demonstrate a linear force–displacement behaviour. OBJs behave almost linearly throughout the duration of the test except for negligible nonlinearity that is observed just prior to the end of the test when failure is to take place. BJs and HJs exhibit similar load bearing capacity performance and endure

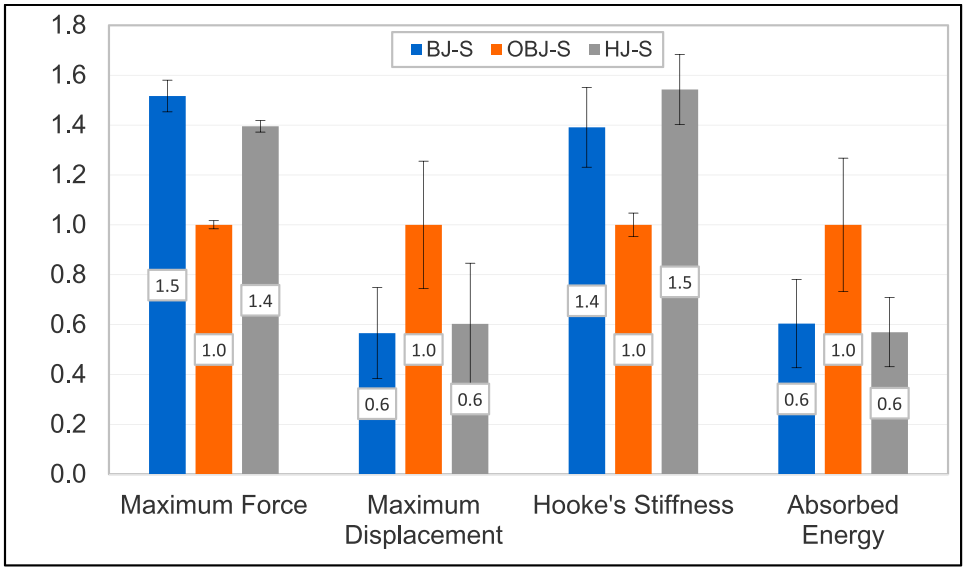

Fig. 9. Comparison of maximum force, displacement, Hooke's stiffness, and absorbed energy of G1 joints (values are normalised to those of OBJ-S). Standard deviation is normalised to the respective average values and shown as error bars.

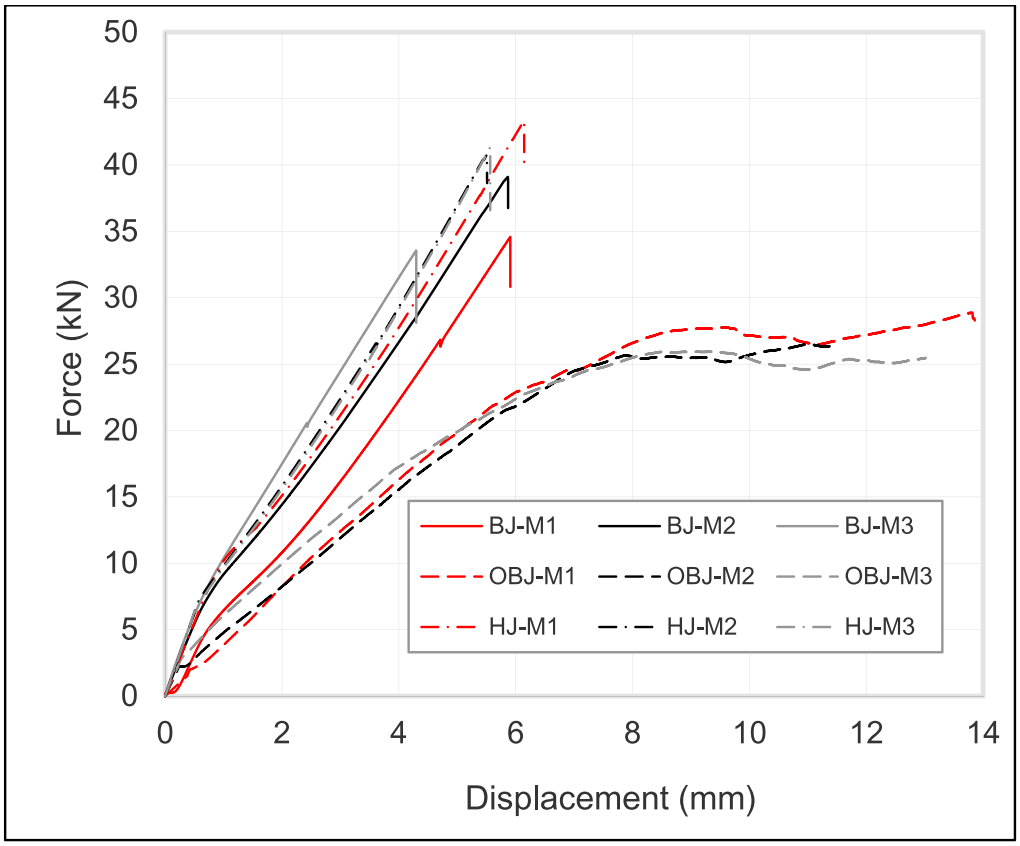

Fig. 10. Force-displacement graph of G2 joints for BJ, OBJ and HJ.

Table 6
Maximum force, displacement, and Hooke's stiffness of G2 joints.

Specimen	Maximum Force (kN)	Maximum Displacement (mm)	Hooke's Stiffness (kN/mm)	Absorbed Energy (J)
BJ-M1	39.10	5.78	5.324	59.61
BJ-M2	34.58	6.15	6.019	49.22
BJ-M3	37.09	4.31	7.662	46.86
Average	36.92	5.41	6.335	51.90
SD	2.26	0.98	1.201	6.78
Average ± SD	36.92 ± 2.26	5.41 ± 0.98	6.335 ± 1.201	51.90 ± 6.78
OBJ-M1	28.87	13.50	4.169	141.20
OBJ-M2	28.57	13.72	3.601	137.60
OBJ-M3	27.76	16.33	3.732	173.78
Average	28.40	14.52	3.834	150.86
SD	0.58	1.57	0.297	19.93
Average ± SD	28.40 ± 0.58	14.52 ± 1.57	3.834 ± 0.297	150.86 ± 19.93
HJ-M1	43.32	6.01	6.160	68.25
HJ-M2	40.79	5.04	6.105	57.68
HJ-M3	41.32	5.12	6.105	58.15
Average	41.81	5.39	6.123	61.36
SD	1.34	0.54	0.032	5.97
Average ± SD	41.81 ± 1.34	5.39 ± 0.54	6.123 ± 0.032	61.36 ± 5.97

1.5 times higher tensile failure load than OBJs. It should be noted that BJs, based on average stiffness values, show a stiffer joint compared to HJs. However, it could be argued that, given the scatter of stiffness values for BJs compared to HJs as reflected in the corresponding standard deviations, the comparison of stiffness for HJs and BJs is rather inconclusive. Comparison of absorbed energy for each joint configuration in G3 shows a different trend from G1 and G2: namely that all joint configurations demonstrate similar energy absorption capability. This is due to the long-bonded overlaps enabling the adhesive in both BJs and HJs to fully develop their strength without premature failure.

In all test groups G1, G2 and G3, the source of force–displacement nonlinearity in OBJs predominantly stems from large displacements and material nonlinearity. Large displacements mostly result from the rotation of the joint, particularly at bolt locations, due to load eccentricity. As the applied load increases, the action line of the load gets closer to the mid-plane of the adherends, and hence its moment arm decreases. Therefore, it is expected that nonlinearities resulting from large deformations are governing the nonlinear behaviour of OBJs at the initial stages of the test. From this perspective, one can conclude that the thickness of both adhesive and adherends will have an impact on the level of nonlinear behaviour of OBJs but this is beyond the scope of current study. Near the final stages of the test, the moment arm (offset between the end forces) decreases. This leads to the reduction of large displacement nonlinearities after which the material nonlinearity and constitutive law of the composite adherends play a key role. In other words, since all the OBJ test specimens started failing first in bearing mode and then shifted to net tension (see section 4.3), material nonlinearity in bearing plays a part in nonlinear behaviour at the final stages of the test. It should be noted that bearing failure mode in this study is the result of joint design as explained in section 3.3.1. This is because bearing failure mode is the preferred failure for aerostructures as it is not abrupt and with a sudden burst of energy.

In BJs and HJs, the geometric nonlinearity is less than OBJs. This is because the distribution of forces in the adherends is spread over the overlap area as opposed to concentrated at bolt locations as in OBJs. The force distribution does not pose significant difference in load offset driven bending moment at the beginning of the test. As the rotation of the joint takes place, both the load offset and adherend forces in the middle of the overlap are less than those of OBJs leading to less rotation and reduced geometric nonlinearity in these joints. Furthermore,

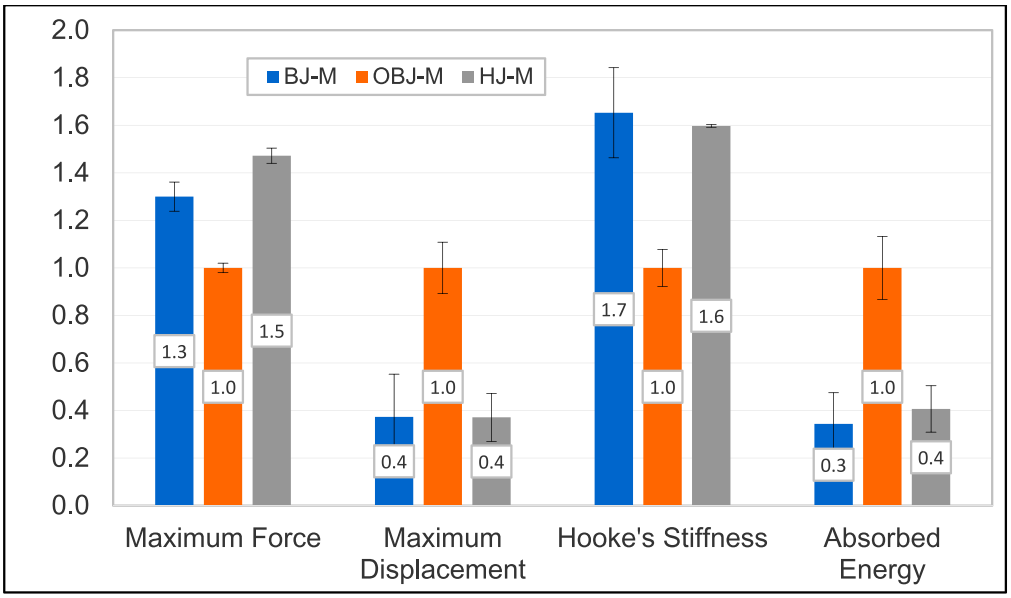

Fig. 11. Comparison of maximum force, displacement, Hooke's stiffness, and absorbed energy of G2 joints (values are normalised to those of OBJ-M). Standard deviation is normalised to the respective average values and shown as error bars.

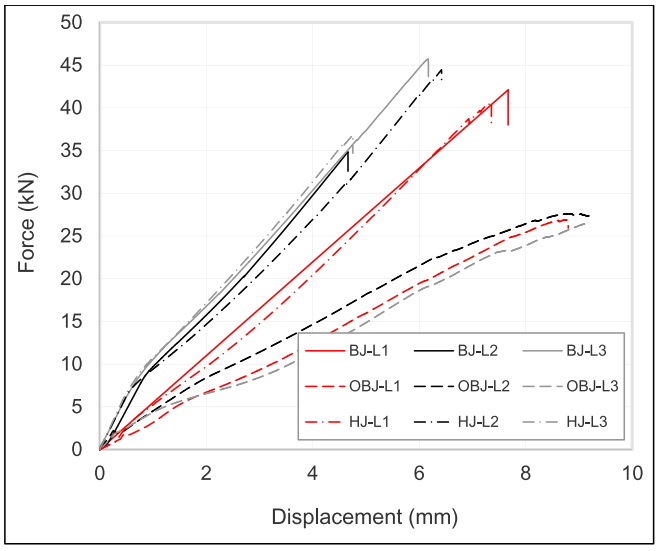

Fig. 12. Force-displacement graph of G3 joints for BJ, OBJ and HJ.

material nonlinearity is considerably less than OBJs as fracture takes place in the adhesive in a brittle and abrupt manner. In other words, once cracks are formed in the brittle adhesive, this leads to sudden fracture of the bond-line and hence that of the joint.

It is interesting to mention that to benefit from HJs, the choice of overlap length is a deciding factor. As mentioned previously, BJs of G1 outperform HJs whereas similar performance is observed for BJs and HJs in G3. However, in G2, HJs outperform BJs. In other words, in this study, large overlaps ($\geq 60t$) and short overlaps ($\leq 35t$) do not take advantage of joint hybridisation while intermediate overlaps ($= 45t$) provide marginal advantage. Overall, BJs show robust performance in single lap shear configuration compared to both HJs and OBJs demonstrating their potential in joining of composite structures. Additionally, one could infer that the HJs would benefit from the merits of the BJs and OBJs. In particular, the expectation is that for the HJs, once the adhesive has failed, there would be a further portion of the load–displacement curve for test groups G2 and G3 like the one observed in OBJs case of test group G1.

Namely, in G1, the curves of the HJs repeat partially those of the OBJs. However, for G2 and G3, the curves of the HJs simply drop after the peak and the joints fail immediately. This is justified as higher overlaps in BJs and HJs lead to higher strength of BJs and HJs as evidenced in the graphs for G1 and G2. These levels of higher loads, far exceeds the bearing strength of OBJs. Hence, in HJs of G2 and G3, when adhesive fails, the existing load is notably greater than the strength of OBJ in bearing failure mode. Therefore, the bolts cannot develop their bearing capability. This leads to HJs performing like BJs for larger overlaps of G2 and G3 with minimal static load bearing benefit from the bolts.

In all test groups, the standard deviation of measured performance parameters for OBJs are lower than BJs and HJs. However, HJs show lower standard deviation compared to BJs. This explains that the quality of OBJs is more consistent than HJs and BJs and the quality of HJs is more consistent than that of BJs. In other words, manufacture of BJs is a less repeatable process than OBJs and HJs.

4.2. *Stress–strain response*

Prior to presenting experimental stress–strain behaviour of joints of this study, it is important to describe the load transfer mechanism in BJs and OBJs as outlined in the literature. Paroissien et al. [47] depicted the theoretical load transfer mechanism for BJs and OBJs as shown in Fig. 14. The load transfer graph shows normalised force within the overlap region at the bottom adherend. If the adherends are infinitely rigid, the shear deformation in the adhesive layer would be constant along the overlap. However, the adherends are deformable and induce a gradient of shear deformation in the adhesive layer along the overlap Fig. 14a. This load transfer mode is continuous because it is performed along the entire overlap. On the other hand, unlike BJs, the load transfer mechanism of OBJs is discrete as it takes place at the fastener location (s).

For research in this paper, stress–strain graphs of adherends for G1, G2 and G3 test configurations are depicted in Fig. 15 to Fig. 19, respectively.

As shown in Fig. 15, for all joint types of G1, average strain using AVE 2 and strain readings of strain gauges SG1, SG2 and SG3 show a linear change of strains with respect to the applied stress. The applied

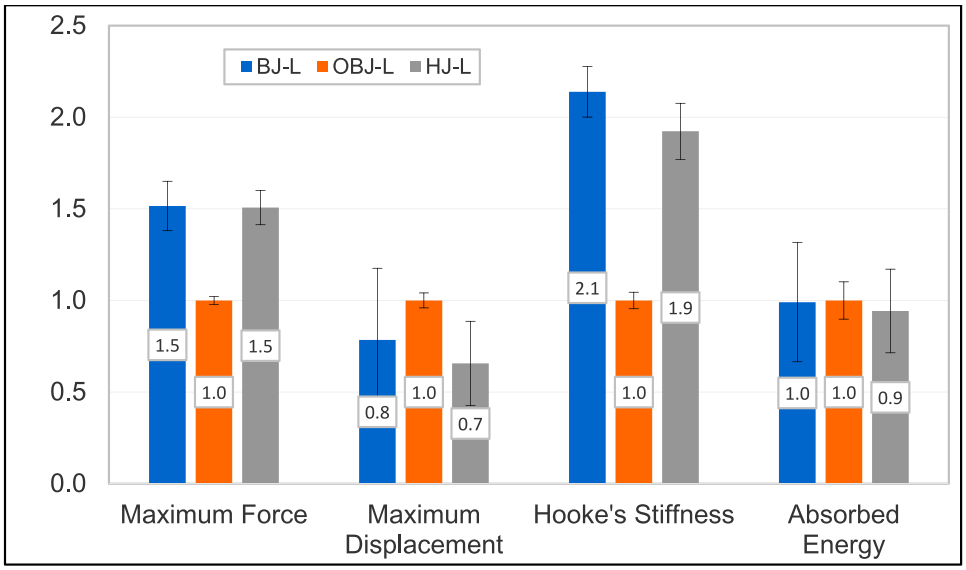

Fig. 13. Comparison of maximum force, displacement, Hooke's stiffness, and absorbed energy of G3 joints (values are normalised to those of OBJ-S). Standard deviation is normalised to their respective average values and shown as error bars.

Table 7
Maximum force, displacement, and Hooke's stiffness of G3 joints.

Specimen	Maximum Force (kN)	Maximum Displacement (mm)	Hooke's Stiffness (kN/mm)	Absorbed Energy (J)
BJ-L1	42.11	9.93	5.483	82.78
BJ-L2	34.85	4.67	7.107	41.92
BJ-L3	45.72	6.18	6.946	74.61
Average	40.89	6.93	6.512	66.44
SD	5.53	2.71	0.895	21.62
Average ± SD	40.89 ± 5.53	6.93 ± 2.71	6.512 ± 0.895	66.44 ± 21.62
OBJ-L1	26.88	8.41	3.170	61.71
OBJ-L2	27.58	9.02	3.069	74.72
OBJ-L3	26.47	9.04	2.896	64.78
Average	26.98	8.82	3.045	67.07
SD	0.56	0.36	0.139	6.80
Average ± SD	26.98 ± 0.56	8.82 ± 0.36	3.045 ± 0.139	67.07 ± 6.80
HJ-L1	40.69	7.04	5.053	71.39
HJ-L2	44.45	5.96	5.694	71.75
HJ-L3	36.82	4.39	6.824	46.53
Average	40.65	5.79	5.857	63.22
SD	3.81	1.33	0.897	14.46
Average ± SD	40.65 ± 3.81	5.79 ± 1.33	5.857 ± 0.897	63.22 ± 14.45

stress is defined as applied force divided by the cross-sectional area of adherend at the loaded end. This result complies with the findings of [32] where strain readings for BJ, OBJs and HJs were linear for quasi-isotropic adherends.

Comparison of Fig. 15a and Fig. 15c shows that BJs experience higher strains at the end and middle of the bottom adherend compared to HJs. In other words, the use of HJs leads to a stiffer joint in which the load transfer occurs faster from the top adherend to the bottom adherend compared to BJs.

Fig. 15b shows that OBJs experience compressive strains at SG3 which could be explained by the fact that bolt compressive bearing stresses are being recorded at this location. On the contrary, SG3 for BJs and HJs are very small and comply with the load transfer mechanism of bonded joints as depicted in Fig. 14a. It is noted that SG3 are not recording exact theoretical strains of zero due to the inability of strain gauges to record strains at exact edge of the overlap region.

To better understand the experimental trend, the parameter β is

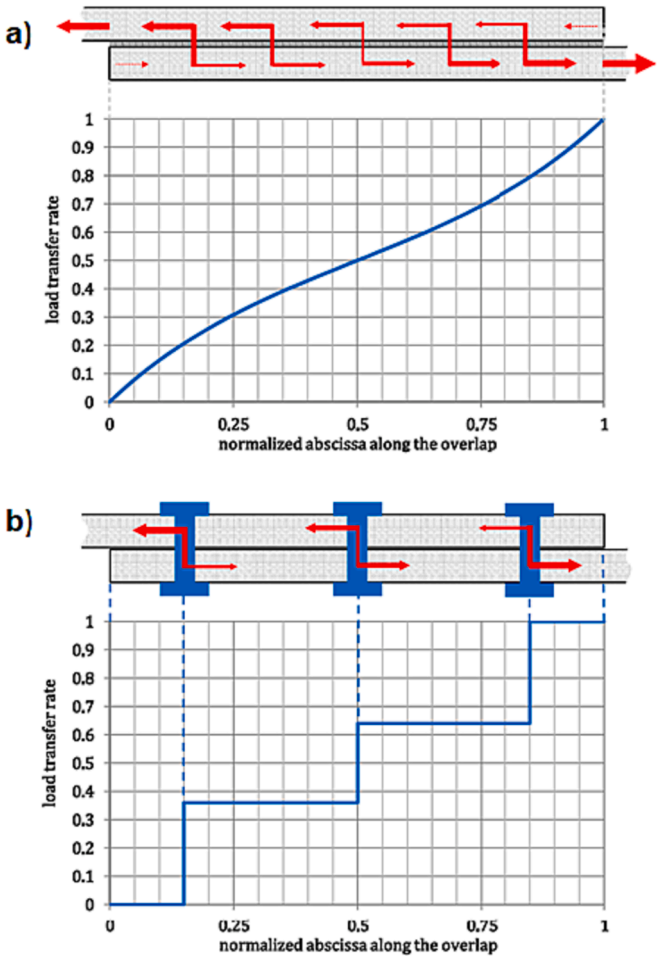

Fig. 14. Load transfer in a single-lap joint, a) BJs, b) OBJs shown for flexible fasteners (taken from [47]).

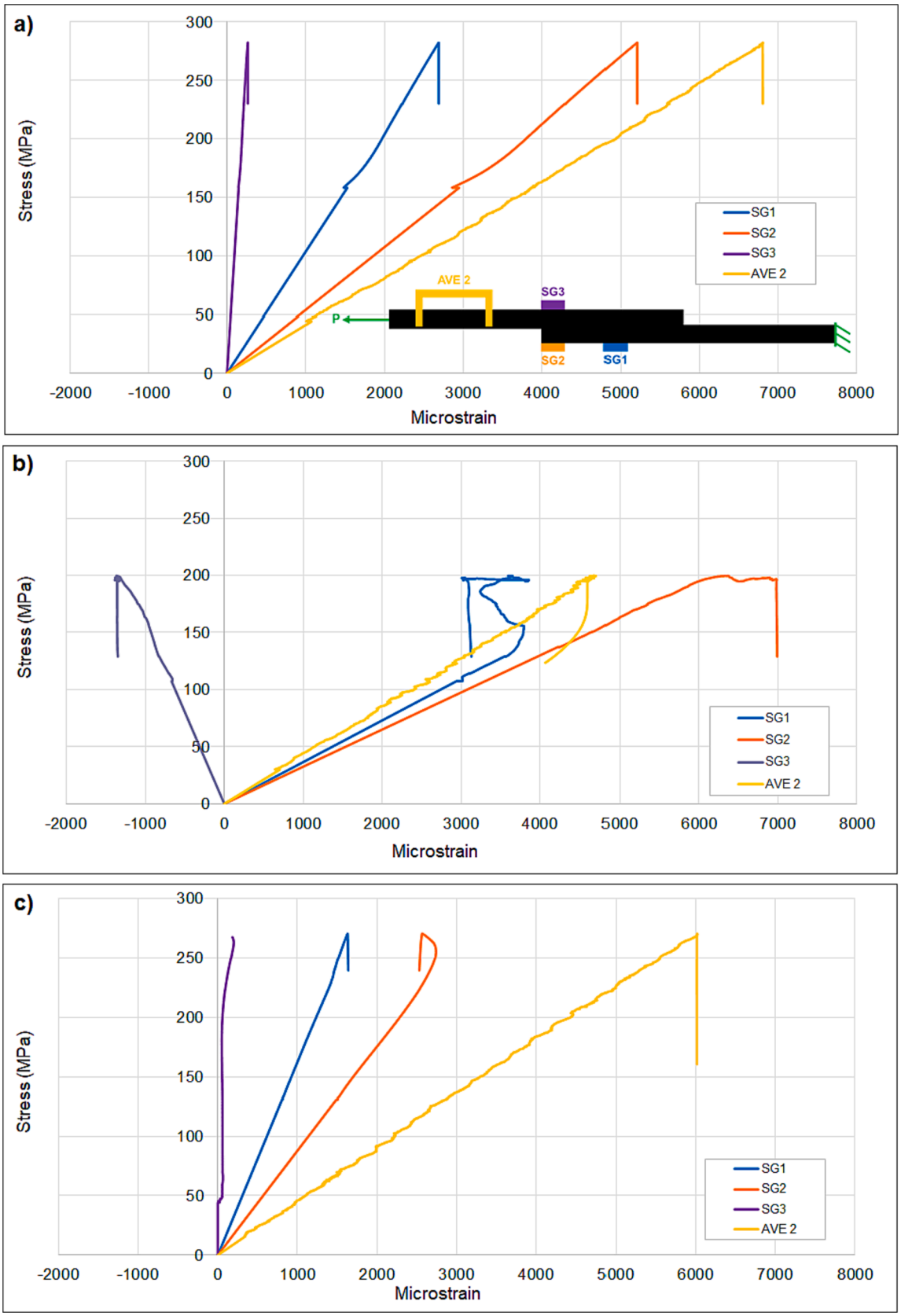

Fig. 15. Stress–strain curves of G1 for a) BJ, b) OBJ and c) HJ.

defined as:

$$\beta = strain\ of\ SG2 - strain\ of\ SG3$$

β is indicative of joint rotation stemming from bending due to load eccentricity. As shown in Fig. 16, β is significantly higher for OBJs compared to either BJs or HJs indicating much higher joint rotation of OBJs compared to the other two joint types. More importantly, as the load increases, β increases commensurately demonstrating higher rotations at the final stages of the loading.

As shown in Fig. 17, for all joint types of G2, average strains using AVE 2 and strain readings of SG1, SG2 and SG3 show a linear change of strains with respect to the applied stress.

Comparison of Fig. 17a and Fig. 17c shows that both BJs and HJs demonstrate similar patterns of stress–strain behaviour but HJs experience higher strains than BJ and OBJ. Again, SG3 in both BJs and HJs show strains of almost zero in line with the load transfer mechanism of BJs as stipulated in [47]. Fig. 17b shows that OBJs experience compressive strains at SG3 which could be explained by the fact that bolt compressive bearing stresses are being recorded at this location as before. Additionally, as shown in Fig. 18, β is significantly higher for OBJs compared to either BJs or HJs indicating much higher joint rotation of OBJs compared to the other two joint types. More importantly, as the load increases, β increases commensurately demonstrating higher rotations at the final stages of the loading.

Based on Fig. 19, for all joint types of G3 test configuration, average strains using AVE 2 and strain readings of SG1, SG2 and SG3 show an almost linear change of strains with respect to the applied stress.

Comparison of Fig. 19a and Fig. 19c shows that HJs experience much higher strains compared to BJs and OBJs. Like G1 and G2 test groups, Fig. 19b shows that OBJs experience compressive strains at SG3. Based on Fig. 20, β is significantly higher for OBJs compared to either BJs or HJs indicating much higher joint rotation of OBJs compared to the other two joint types. More importantly, as the load increases, β increases commensurately demonstrating higher rotations at the final stages of the loading. It is worth noting that β is higher for HJs than BJs showing that HJs experience higher joint rotation than BJs. OBJs fail much earlier than BJs and HJs and as such experience much lower strains.

4.3. Failure modes

The failure modes of BJs, OBJs and HJs for test configurations G1, G2 and G3 are shown and colour coded in Fig. 21, Fig. 22 and Fig. 23, respectively.

Based on Fig. 21 for G1, the BJs fail in cohesive failure (see Fig. 21a where the white lines show the boundary between the residue of adhesive and failed adhesive on the adherend). The OBJs fail under combined bearing and net tension mode (Fig. 21b). In other words, the fastener hole experiences significant bearing deformation, after which net tension failure of specimen takes place. The cross-sectional view of the specimen reveals some degrees of matrix cracking and delamination around the fastener hole (Section A-A of Fig. 21b). Unlike OBJs, HJs experience minor bearing deformation at the fastener hole but predominantly fail due to cohesive failure (Fig. 21c). Once the adhesive completely fails, the existing load is redistributed into the fasteners leading to bearing and net tension failure of the adherends.

As shown in Fig. 22a, BJs of G2 test configuration still fail in cohesive failure. This is expected as both shear and peel stresses are higher in those regions leading to earlier failure in these areas. The OBJs undergo notable bearing deformation albeit less than that of OBJs of G1 specimens (Fig. 22b) and finally fail under net tension failure mode. Like G1 configuration, HJs experience both matrix cracking and delamination. However, HJs demonstrate partial cohesive failure (Fig. 22c). In other words, the bonded zone around the fastener hole close to the fixed end fails whereas the remaining bonded areas (particularly the area close to the loaded end) stay intact. This observation confirms the finding of Fu et al. [18] in which bolts are reported to reduce peel stresses and arrest cracking in the adhesive and, hence, delay the failure of adhesive and minimise the progression of adhesive failure. Additionally, HJs see bearing deformation of a fastener hole (less than that of OBJs) and do experience fibre fracture and eventually net tension failure.

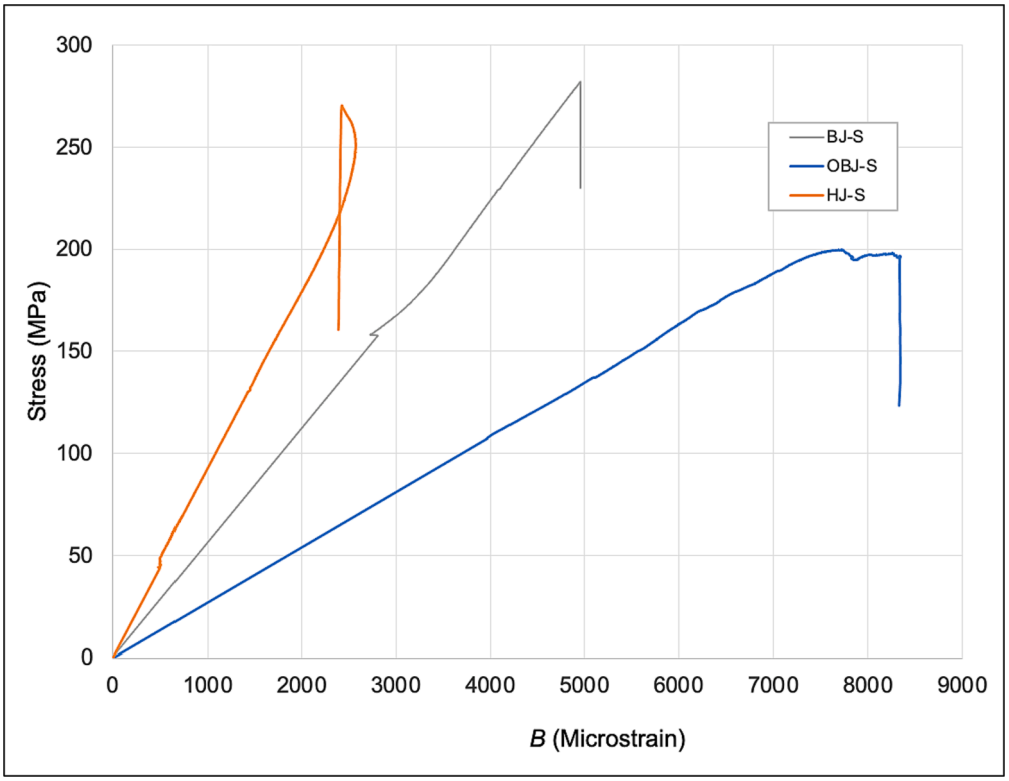

Fig. 16. Parameter β of G1 for BJ, OBJ and HJ.

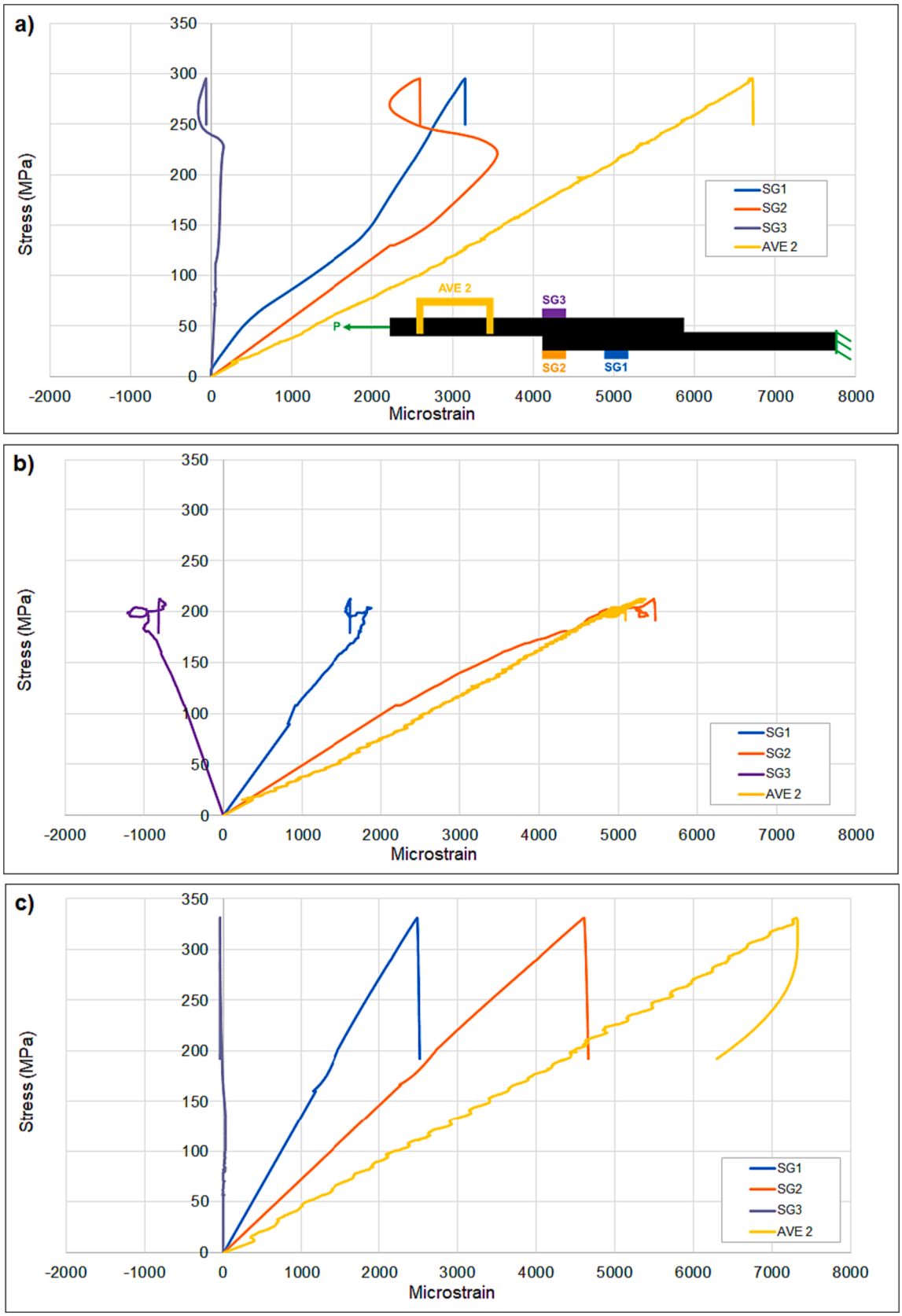

Fig. 17. Stress–strain curves of G2 for a) BJ, b) OBJ and c) HJ.

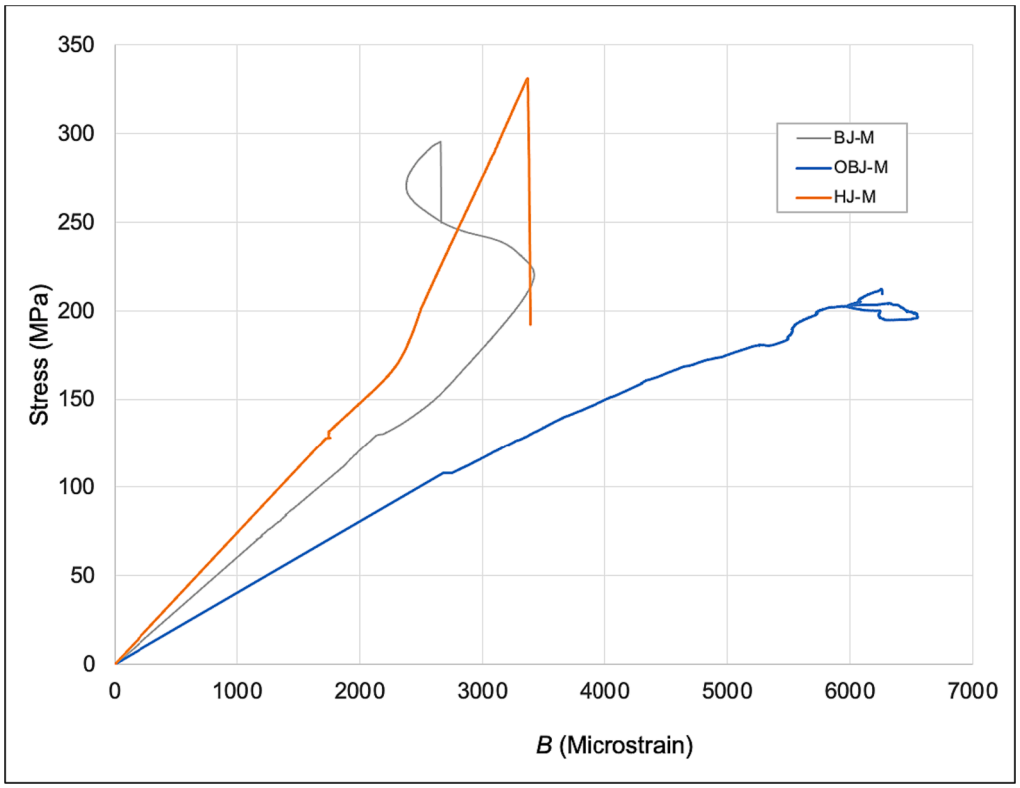

Fig. 18. Parameter β of G2 for BJ, OBJ and HJ.

Based on Fig. 23a, BJs of G3 test configuration fail in cohesive failure with the failed region close to the edges of the overlap nearer to the loaded end. This observation is the same as what is seen for G1 and G2. The OBJs go through notable bearing deformation (Fig. 23b) and finally fail under net tension failure mode. HJs experience matrix cracking but there is no evidence of adherend delamination. Like G2, HJs demonstrate partial cohesive failure (Fig. 22c). Namely, the bonded zone around the fastener hole close to the fixed end fails whereas the remaining bonded areas, particularly the area close to the loaded end, stays intact. Additionally, HJs see bearing deformation around fastener holes (considerably less than that of OBJs) and do experience fibre fracture and, eventually, net tension failure.

The above-mentioned comparison of failure modes of G1, G2 and G3 indicate that for small overlaps, BJs behave similarly and fail in cohesive failure mode. As the length of overlap increases, the failure mode of OBJs does not change significantly although delamination failure mode diminishes. For all overlap lengths, there is significant bearing deformation at one of the fastener holes only which then leads to fibre fracture and net tension failure of adherends. On the contrary, HJs predominantly fail in cohesive failure for small overlap length with negligible bearing deformation. However, as the overlap length increases cohesive failure is followed by both bearing and net tension failure of adherends.

5. Conclusions

To carry out comparative performance study of bonded joints (BJs), only bolted joints (OBJs) and hybrid bonded-bolted joints (HJs) three test configurations were considered. The test configurations were based on overlap length of two quasi-isotropic composite adherends made of twill woven fabrics, i.e. short (G1), medium (G2) and long (G3) overlap. In each test configuration, three specimens of BJs, OBJs and HJs (total of 9 specimens for each test group) were tested for statistical representation. The principal findings are as follows:

- Force-displacement data revealed a linear behaviour for BJs and HJs whereas OBJs behaved nonlinearly. Overall, HJs demonstrated higher failure load than BJs and OBJs except for G1 where BJs outperformed. In all test groups, OBJs performed poorly in most characteristic behaviour measured, i.e. failure load and Hooke's stiffness. However, due to bearing deformation at bolt hole locations, OBJs experienced higher failure displacements than BJs and HJs. This led to a desirable energy absorption mechanism compared to that of HJs and BJs thanks to bearing failure mode (despite much lower failure load in OBJs). It was revealed that increasing the overlap length worked to the benefit of BJs. However, for medium length overlap HJs showed better performance. In all test groups, the standard deviation of measured characteristic parameters was the least for OBJs then HJs and BJs. This suggests more consistent quality of OBJs compared to HJs and BJs and more consistent quality of HJs than BJs.
- Stress–strain behaviours showed a linear behaviour for all test groups with significant joint rotation for OBJs compared to BJs and HJs. The qualitative comparison of load path matched reasonably well with theoretical expectation.
- The failure mechanism studies showed that BJs failed in cohesive failure for all test groups. OBJs failed in bearing leading to net tension failure with significant fibre fracture emanating from the edge of the fastener hole. OBJs experienced matrix cracking and delamination at bolt hole locations. On the other hand, HJs experienced considerably less bearing failure at bolt holes due to the load bearing contribution of the adhesives.

In future work, it is hoped to investigate the effects of load eccentricity in detail using 3D FEA and the experimental results of the current study. Further experimental work using DIC technique (like [28]) is required to fully understand the effects of load eccentricity on the behaviour of hybrid joints. Moreover, the use of ductile adhesive and its effect on load sharing between bolts and adhesive need to be studied both experimentally and numerically. Furthermore, the behaviour of

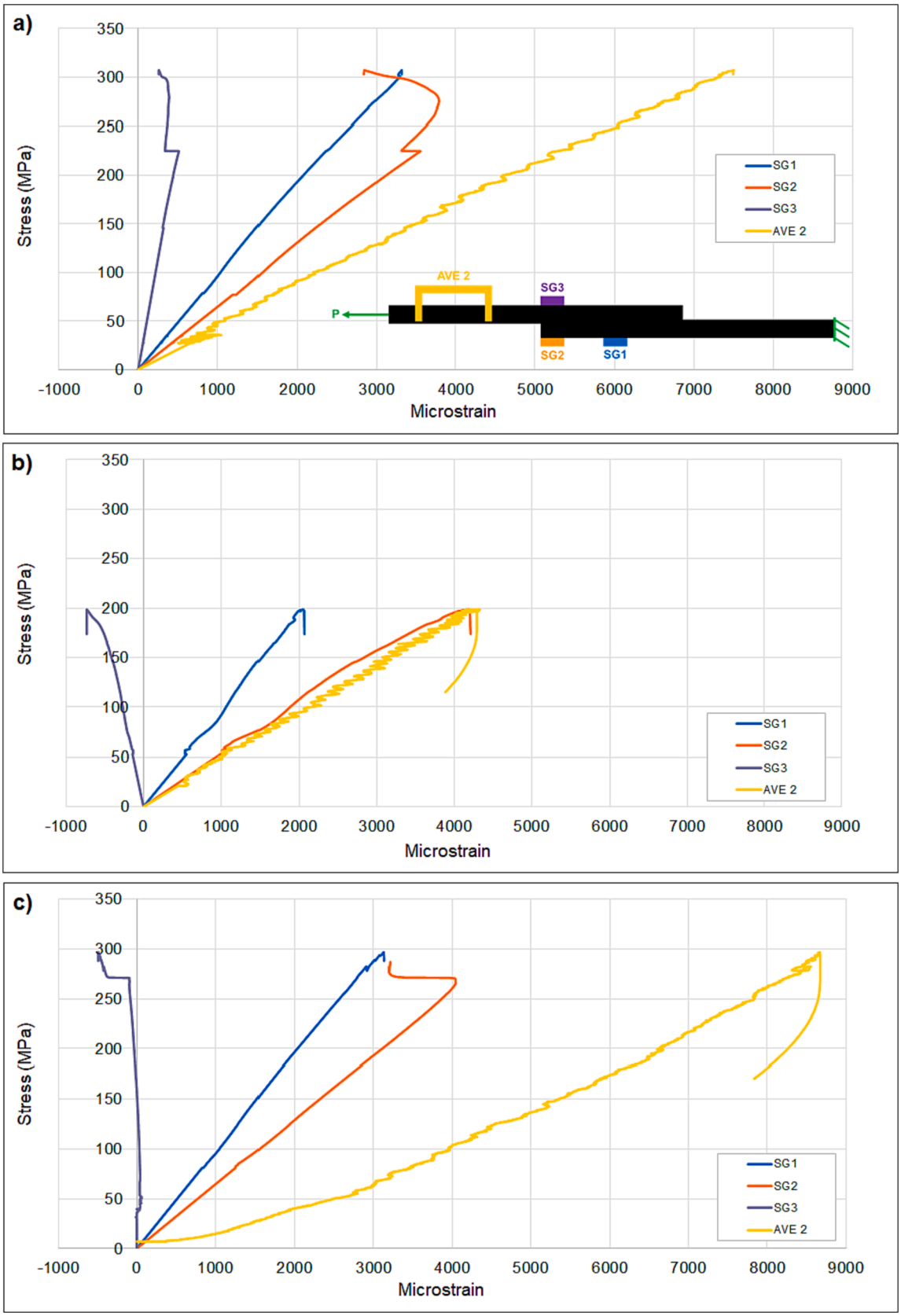

Fig. 19. Stress–strain curves of G3 for a) BJ, b) OBJ and c) HJ.

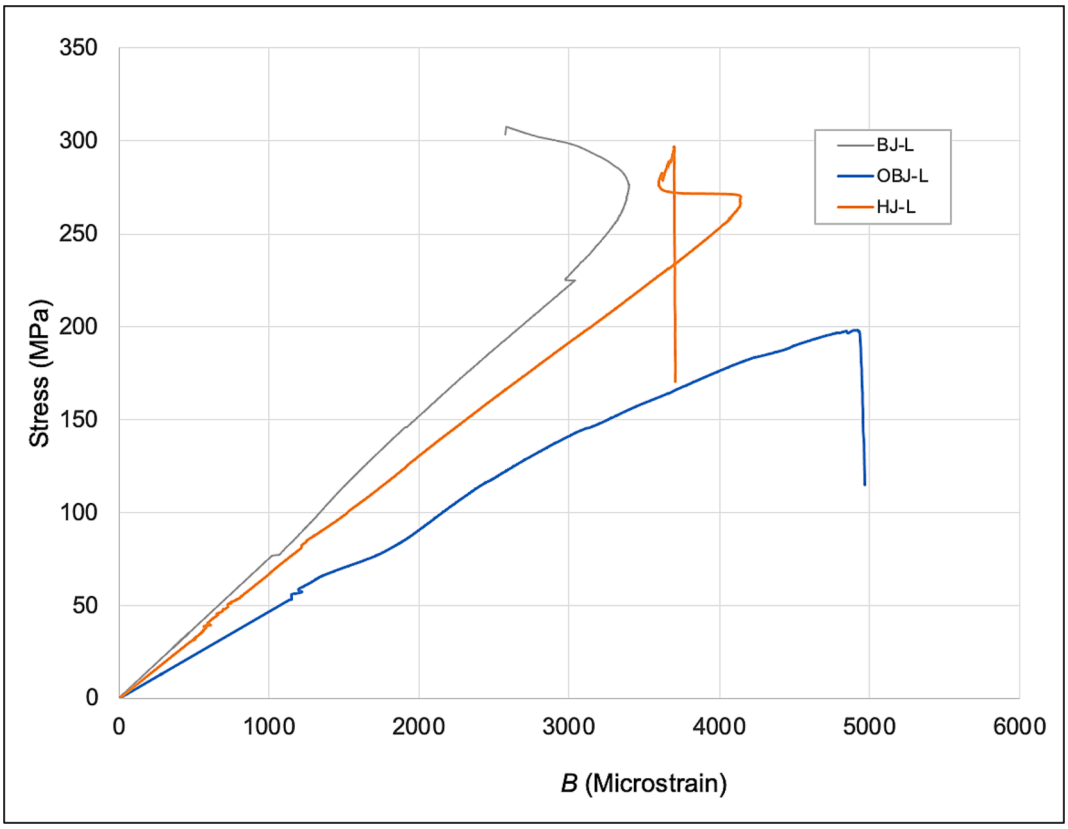

Fig. 20. Parameter β of G3 for BJ, OBJ and HJ.

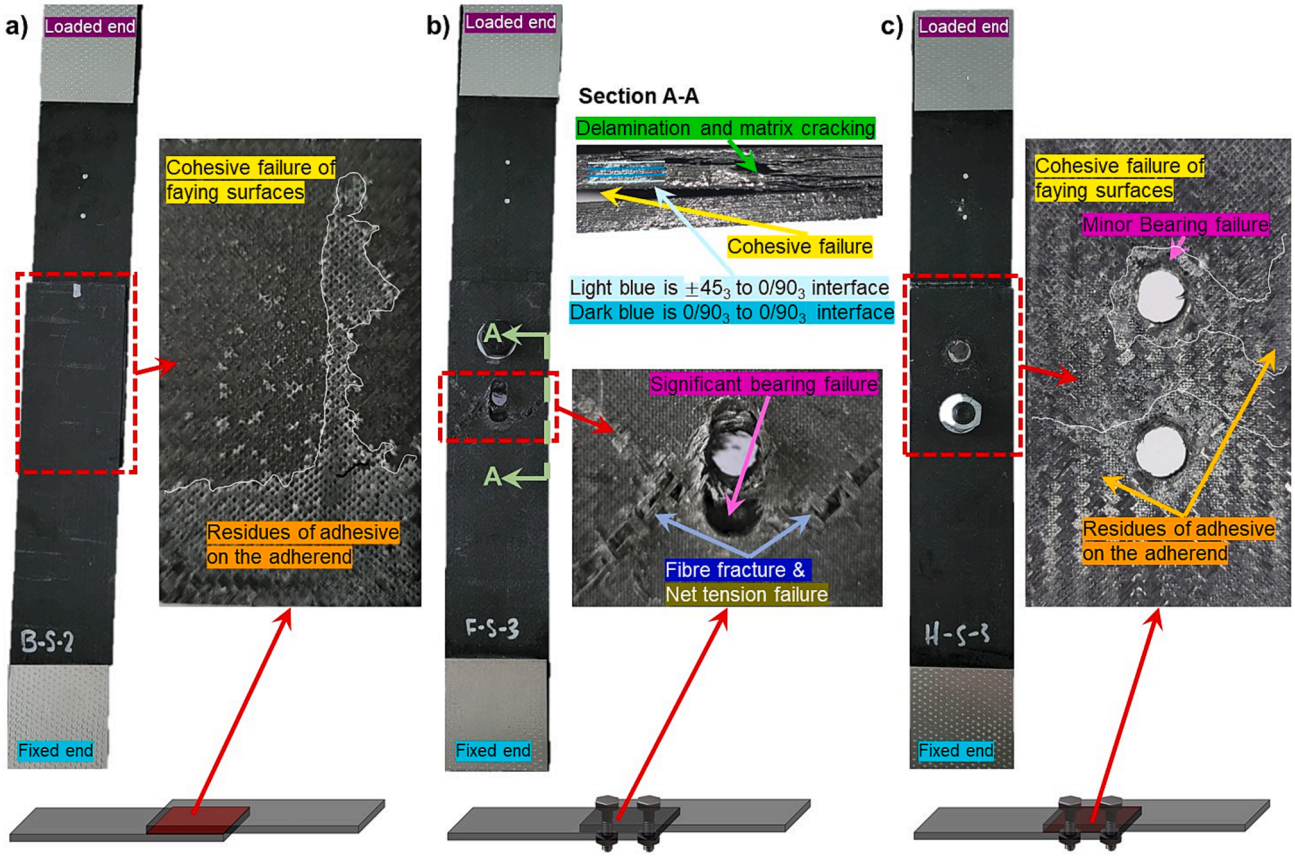

Fig. 21. Failure modes of G1 for a) BJs, b) OBJs and c) HJs.

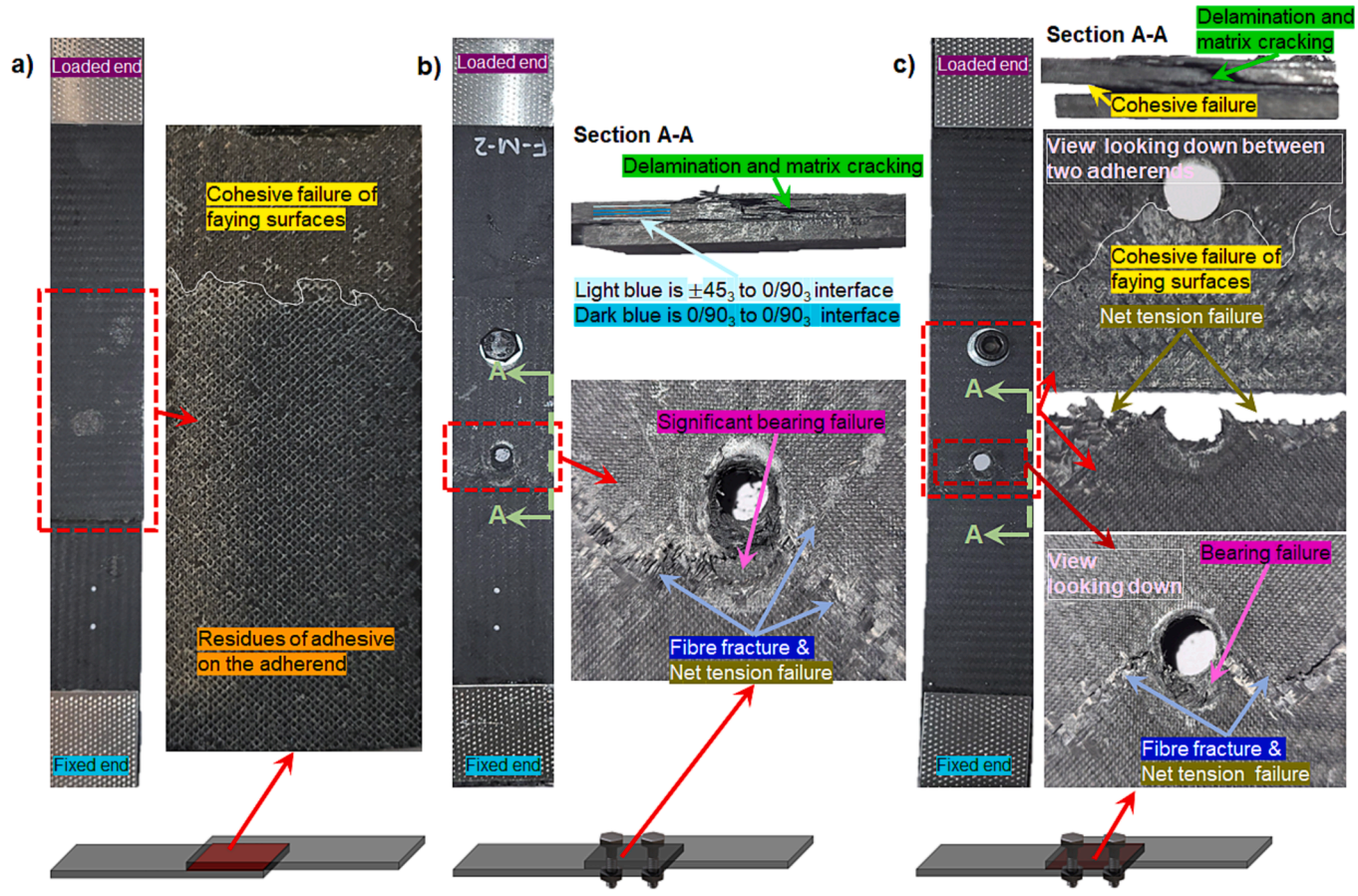

Fig. 22. Failure modes of G2 for a) BJs, b) OBJs and c) HJs.

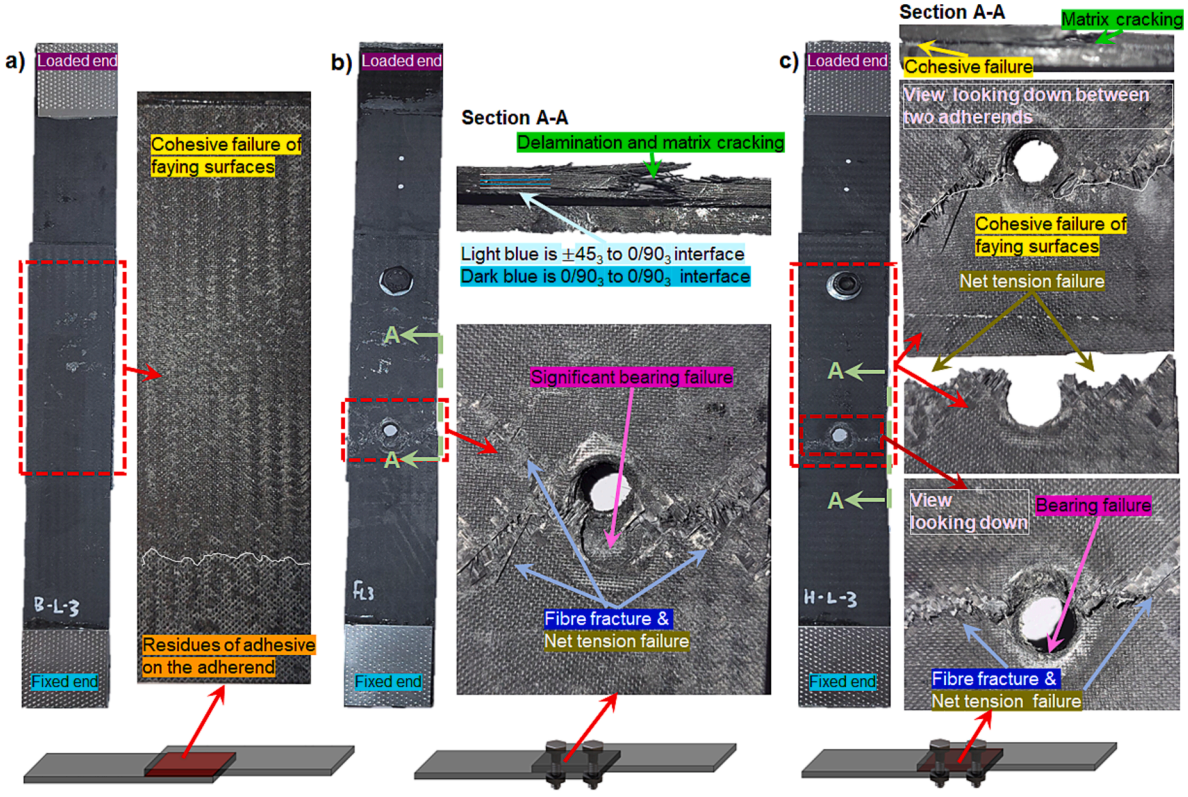

Fig. 23. Failure modes of G3 for a) BJs, b) OBJs and c) HJs.

HJs need to be studied in other joint configurations such as Double-Lap Shear Joints (DLSJ).

CRediT authorship contribution statement

Mahdi Damghani: Writing – review & editing, Writing – original draft, Visualization, Validation, Supervision, Software, Resources, Project administration, Methodology, Investigation, Funding acquisition, Formal analysis, Data curation, Conceptualization. **Mohammad Saad Khan:** Investigation, Data curation. **Gary A. Atkinson:** Writing – review & editing.

Declaration of competing interest

The authors declare that they have no known competing financial interests or personal relationships that could have appeared to influence the work reported in this paper.

Data availability

Data will be made available on request.

References

[1] Alam P, Mamalis D, Robert C, Floreani C, Ó Brádaigh CM. The fatigue of carbon fibre reinforced plastics - A review. Compos B Eng 2019;166:555–79. https://doi.org/https://doi.org/10.1016/j.compositesb.2019.02.016.

[2] Damghani M, Bolanos S, Chahar A, Matthews J, Atkinson GA, Murphy A, et al. Design, novel quality check and experimental test of an original variable length stepped scarf repair scheme. Compos B Eng 2022;230:109542. https://doi.org/10.1016/J.COMPOSITESB.2021.109542.

[3] Damghani M, Bakunowicz J, Murphy A. Understanding the influence of laminate stacking sequence on strain/stress concentrations in thin laminates at repair holes with large scarf angles. J Compos Mater 2019;53:4273–84. https://doi.org/10.1177/0021998319855772.

[4] Dauguet M, Mantaux O, Perry N, Zhao YF. Recycling of CFRP for high value applications: Effect of sizing removal and environmental analysis of the supercritical fluid Solvolysis. Procedia CIRP 2015;29:734–9. https://doi.org/10.1016/j.procir.2015.02.064.

[5] Damghani M, Saddler J, Sammon E, Atkinson GA, Matthews J, Murphy A. An experimental investigation of the impact response and Post-impact shear buckling behaviour of hybrid composite laminates. Compos Struct 2023;305:116506. https://doi.org/10.1016/j.compstruct.2022.116506.

[6] Damghani M, Ersoy N, Piorkowski M, Murphy A. Experimental evaluation of residual tensile strength of hybrid composite aerospace materials after low velocity impact. Compos B Eng 2019;179:107537.

[7] Fotouhi S, Khayatzadeh S, Pui Xia W, Damghani M, Bodaghi M, Fotouhi M. Detection of barely visible impact damage in polymeric laminated composites using a biomimetic tactile whisker. Polymers (Basel) 2021;20:3587. https://doi.org/10.3390/polym13203587.

[8] Zhang S, Zhao D. Aerospace Material Handbook. CRC Press; 2012.

[9] Campbell FC. Chapter 8 - Adhesive Bonding and Integrally Cocured Structure. In: Campbell FCBT-MT for ASM, editor., Oxford: Elsevier Science; 2006, p. 369–418. https://doi.org/https://doi.org/10.1016/B978-185617495-4/50008-1.

[10] da Silva LFM, Ochsner A, Adams R. Handbook of Adhesion Technology. Springer, Cham; 2011. https://doi.org/https://doi.org/10.1007/978-3-319-42087-5.

[11] Budhe S, Banea MD, de Barros S, da Silva LFM. An updated review of adhesively bonded joints in composite materials. Int J Adhes Adhes 2017;72:30–42. https://doi.org/10.1016/j.ijadhadh.2016.10.010.

[12] Sorrentino L, Parodo G, Turchetta S. CFRP laser texturing to increase the adhesive bonding: morphological analysis of treated surfaces. J Adhes 2021;97:1322–35. https://doi.org/10.1080/00218464.2020.1758074.

[13] Arenas JM, Narbón JJ, Alía C. Optimum adhesive thickness in structural adhesives joints using statistical techniques based on Weibull distribution. Int J Adhes Adhes 2010;30:160–5. https://doi.org/10.1016/j.ijadhadh.2009.12.003.

[14] Chowdhury N, Chiu WK, Wang J, Chang P. Static and fatigue testing thin riveted, bonded and hybrid carbon fiber double lap joints used in aircraft structures. Compos Struct 2015;121:315–23. https://doi.org/10.1016/j.compstruct.2014.11.004.

[15] Damghani M, Harrison C, Kennedy D. The effects of composite laminate stiffness and loading on stress resultant concentration factor around a hole. Proc Inst Mech Eng C J Mech Eng Sci 2018;232:0954406218755187. https://doi.org/10.1177/0954406218755187.

[16] Galińska A. Mechanical joining of fibre reinforced polymer composites to metals—A review. Part I: Bolted joining. Polymers (Basel) 2020:12. https://doi.org/10.3390/polym12102252.

[17] Jeevi G, Nayak SK, Abdul KM. Review on adhesive joints and their application in hybrid composite structures. J Adhes Sci Technol 2019;33:1497–520. https://doi.org/10.1080/01694243.2018.1543528.

[18] Fu M, Mallick PK. Fatigue of hybrid (adhesive/bolted) joints in SRIM composites. Int J Adhes Adhes 2001;21:145–59. https://doi.org/10.1016/S0143-7496(00)00047-6.

[19] Kelly G. Load transfer in hybrid (bonded/bolted) composite single-lap joints. Compos Struct 2005;69:35–43. https://doi.org/10.1016/j.compstruct.2004.04.016.

[20] Matsuzaki R, Shibata M, Todoroki A. Improving performance of GFRP/aluminum single lap joints using bolted/co-cured hybrid method. Compos Part A Appl Sci Manuf 2008;39:154–63. https://doi.org/10.1016/j.compositesa.2007.11.009.

[21] Esmaeili F, Zehsaz M, Chakherlou TN. Investigation the effect of tightening torque on the fatigue strength of double lap simple bolted and hybrid (bolted–bonded) joints using volumetric method. Mater Des 2014;63:349–59. https://doi.org/10.1016/j.matdes.2014.06.021.

[22] Bodjona K, Raju K, Lim G-H, Lessard L. Load sharing in single-lap bonded/bolted composite joints. Part I: Model development and validation. Compos Struct 2015;129:268–75. https://doi.org/10.1016/j.compstruct.2015.04.040.

[23] Bodjona K, Lessard L. Load sharing in single-lap bonded/bolted composite joints. Part II: Global sensitivity analysis. Compos Struct 2015;129:276–83. https://doi.org/10.1016/j.compstruct.2015.03.069.

[24] Chowdhury NM, Chiu WK, Wang J, Chang P. Experimental and finite element studies of bolted, bonded and hybrid step lap joints of thick carbon fibre/epoxy panels used in aircraft structures. Compos B Eng 2016;100:68–77. https://doi.org/10.1016/j.compositesb.2016.06.061.

[25] Lopez-Cruz P, Laliberté J, Lessard L. Investigation of bolted/bonded composite joint behaviour using design of experiments. Compos Struct 2017;170:192–201. https://doi.org/10.1016/j.compstruct.2017.02.084.

[26] El Zaroug M, Kadioglu F, Demiral M, Saad D. Experimental and numerical investigation into strength of bolted, bonded and hybrid single lap joints: Effects of adherend material type and thickness. Int J Adhes Adhes 2018;87:130–41. https://doi.org/10.1016/j.ijadhadh.2018.10.006.

[27] Li X, Tan Z, Wang L, Zhang J, Xiao Z, Luo H. Experimental investigations of bolted, adhesively bonded and hybrid bolted/bonded single-lap joints in composite laminates. Mater Today Commun 2020;24:101244. https://doi.org/10.1016/j.mtcomm.2020.101244.

[28] Selahi E, Chowdhury NM, Chiu WK, Wang J, Chang P, Jiang L, et al. 3D-DIC strain field measurements in bolted and hybrid bolted-bonded joints of woven carbon-epoxy composites. Compos B Eng 2022;69:108897. https://doi.org/10.1016/j.compositesb.2021.108875.

[29] Romanov VS, Heidari-Rarani M, Lessard L. A parametric study on static behavior and load sharing of multi-bolt hybrid bonded/bolted composite joints. Compos B Eng 2021;217:108897. https://doi.org/10.1016/j.compositesb.2021.108897.

[30] Jiang L, Dong D, Xiao S, Chen D, Yang B, Yang G, et al. Experiment and simulation study on bonded, bolted and hybrid bolted/bonded joints of textile CFRP using bimodulus constitutive model. Int J Adhes Adhes 2022;116:103154. https://doi.org/10.1016/j.ijadhadh.2022.103154.

[31] Li X, Xu B, Hong Y, Luo H. A detailed experimental parametric analysis of bolted and hybrid bolted/bonded composite joints. J Appl Polym Sci 2023;140:e53394.

[32] Jiang L, Xiao S, Dong D, Yang B, Chen D, Yang G, et al. Experimental study of bonded, bolted, and hybrid braided CFRP joints with different stacking sequences and lapping patterns. Thin-Walled Struct 2022;177:109408. https://doi.org/10.1016/j.tws.2022.109408.

[33] Bodjona K, Lessard L. Hybrid bonded-fastened joints and their application in composite structures: A general review. J Reinf Plast Compos 2016;35:764–81. https://doi.org/10.1177/0731684415627296.

[34] Damghani M, Wallis C, Bakunowicz J, Murphy A. Using laminate hybridisation (CFRP-GFRP) and shaped CFRP plies to increase plate post-buckling strain to failure under shear loading. Thin-Walled Struct 2021;162:107543. https://doi.org/10.1016/j.tws.2021.107543.

[35] Damghani M, Pir RA, Murphy A, Fotouhi M. Experimental and numerical study of hybrid (CFRP-GFRP) composite laminates containing circular cut-outs under shear loading. Thin-Walled Struct 2022;179:109752. https://doi.org/10.1016/j.tws.2022.109752.

[36] Goh JY, Georgiadis S, Orifici AC, Wang CH. Effects of bondline flaws on the damage tolerance of composite scarf joints. Compos Part A Appl Sci Manuf 2013;55:110–9. https://doi.org/10.1016/j.compositesa.2013.07.017.

[37] Ghazali E, Dano M-L-L, Gakwaya A, Amyot C-O-O. Experimental and numerical studies of stepped-scarf circular repairs in composite sandwich panels. Int J Adhes Adhes 2018;82:41–9. https://doi.org/10.1016/j.ijadhadh.2017.12.008.

[38] Kim MK, Elder DJ, Wang CH, Feih S. Interaction of laminate damage and adhesive disbonding in composite scarf joints subjected to combined in-plane loading and impact. Compos Struct 2012;94:945–53. https://doi.org/10.1016/j.compstruct.2011.10.017.

[39] Khashaba UA, Najjar IMR. Adhesive layer analysis for scarf bonded joint in CFRE composites modified with MWCNTs under tensile and fatigue loads. Compos Struct 2018;184:411–27. https://doi.org/10.1016/J.COMPSTRUCT.2017.09.095.

[40] Cognard JY, Sohier L, Davies P. A modified Arcan test to analyze the behavior of composites and their assemblies under out-of-plane loadings. Compos Part A Appl Sci Manuf 2011;42:111–21. https://doi.org/10.1016/J.COMPOSITESA.2010.10.012.

[41] Kodur V, Yahyai M, Rezaeian A, Eslami M, Poormohamadi A. Residual mechanical properties of high strength steel bolts subjected to heating-cooling cycle. J Constr Steel Res 2017;131:122–31. https://doi.org/10.1016/j.jcsr.2017.01.007.

[42] Hu Y, Shen L, Nie S, Yang B, Sha W. FE simulation and experimental tests of high-strength structural bolts under tension. J Constr Steel Res 2016;126:174–86. https://doi.org/10.1016/j.jcsr.2016.07.021.

[43] Kassapoglou C. Design and Analysis of Composite Structures: With Applications to Aerospace Structures, 2nd Edition. 2nd ed. John Wiley & Sons Ltd; 2013. https://doi.org/10.1002/9781118536933.
[44] Raju KP, Bodjona K, Lim G-H, Lessard L. Improving load sharing in hybrid bonded/bolted composite joints using an interference-fit bolt. Compos Struct 2016;149:329–38. https://doi.org/10.1016/j.compstruct.2016.04.025.
[45] Wei J, Jiao G, Jia P, Huang T. The effect of interference fit size on the fatigue life of bolted joints in composite laminates. Compos B Eng 2013;53:62–8. https://doi.org/10.1016/j.compositesb.2013.04.048.
[46] Abdullah MS, Abdullah AB, Samad Z. 1 - Review of hole-making technology for composites. In: Abdullah AB, Sapuan SM, editors. Hole-Making and Drilling Technology for Composites, Woodhead Publishing; 2019, p. 1–15. https://doi.org/https://doi.org/10.1016/B978-0-08-102397-6.00001-5.
[47] Paroissien E, Lachaud F, Schwartz S. Modelling load transfer in single-lap adhesively bonded and hybrid (bolted / bonded) joints. Prog Aerosp Sci 2022;130:100811. https://doi.org/10.1016/J.PAEROSCI.2022.100811.